Early diagenesis in the sediments of the Congo deep-sea fan dominated by massive terrigenous deposits: Part II - Iron-sulfur coupling

Martial Taillefert, Jordon S. Beckler, Cecile Cathalot, Panagiotis Michalopoulos, Rudolph Corvaisier, Nicole Kiriazis, Jean-Claude Caprais, Lucie Pastor, Christophe Rabouille

▶ **To cite this version:**

Martial Taillefert, Jordon S. Beckler, Cecile Cathalot, Panagiotis Michalopoulos, Rudolph Corvaisier, et al.. Early diagenesis in the sediments of the Congo deep-sea fan dominated by massive terrigenous deposits: Part II - Iron-sulfur coupling. Deep Sea Research Part II: Topical Studies in Oceanography, 2017, 142, pp.151-166. 10.1016/j.dsr2.2017.06.009 . hal-02613239

HAL Id: hal-02613239
https://hal.science/hal-02613239v1

Submitted on 19 May 2020

HAL is a multi-disciplinary open access archive for the deposit and dissemination of scientific research documents, whether they are published or not. The documents may come from teaching and research institutions in France or abroad, or from public or private research centers.

L'archive ouverte pluridisciplinaire **HAL**, est destinée au dépôt et à la diffusion de documents scientifiques de niveau recherche, publiés ou non, émanant des établissements d'enseignement et de recherche français ou étrangers, des laboratoires publics ou privés.

Deep-sea Research Part Ii-topical Studies In Oceanography
August 2017, Volume 142 Pages 151-166
http://dx.doi.org/10.1016/j.dsr2.2017.06.009
http://archimer.ifremer.fr/doc/00389/50068/
© 2017 Elsevier Ltd. All rights reserved.

Achimer
http://archimer.ifremer.fr

Early diagenesis in the sediments of the Congo deep-sea fan dominated by massive terrigenous deposits: Part II – Iron–sulfur coupling

Taillefert Martial [1, *], Beckler Jordon S. [1, 2], Cathalot Cecile [3], Michalopoulos Panagiotis [4], Corvaisier Rudolph [5], Kiriazis Nicole [1], Caprais Jean-Claude [6], Pastor Lucie [6], Rabouille Christophe [7]

[1] Georgia Inst Technol, Sch Earth & Atmospher Sci, Atlanta, GA 30332 USA.
[2] Mote Marine Lab, Ocean Technol Res Program, Sarasota, FL 34236 USA.
[3] IFREMER, Ctr Bretagne, REM GM Lab Cycles Geochim & Ressources, F-29280 Plouzane, France.
[4] Hellen Ctr Marine Res, Inst Oceanog, Anavyssos Attiki, Greece.
[5] Inst Univ Europeen Mer, CNRS, UBO, Lab Sci Environm Marin, F-29280 Plouzane, France.
[6] IFREMER, Ctr Bretagne, REM EEP Lab Environm Profond, F-29280 Plouzane, France.
[7] CEA, CNRS, UVSQ, Lab Sci Climat & Environm, F-91198 Gif Sur Yvette, France.

* Corresponding author : Martial Taillefert, email address : mtaillef@eas.gatech.edu

Abstract :

Deep-sea fans are well known depot centers for organic carbon that should promote sulfate reduction. At the same time, the high rates of deposition of unconsolidated metal oxides from terrigenous origin may also promote metal-reducing microbial activity. To investigate the eventual coupling between the iron and sulfur cycles in these environments, shallow sediment cores (< 50 cm) across various channels and levees in the Congo River deep-sea fan (~5000 m) were profiled using a combination of geochemical methods. Interestingly, metal reduction dominated suboxic carbon remineralization processes in most of these sediments, while dissolved sulfide was absent. In some 'hotspot' patches, however, sulfate reduction produced large sulfide concentrations which supported chemosynthetic-based benthic megafauna. These environments were characterized by sharp geochemical boundaries compared to the iron-rich background environment, suggesting that FeS precipitation efficiently titrated iron and sulfide from the pore waters. A companion study demonstrated that methanogenesis was active in the deep sediment layers of these patchy ecosystems, suggesting that sulfate reduction was promoted by alternative anaerobic processes. These highly reduced habitats could be fueled by discrete, excess inputs of highly labile natural organic matter from Congo River turbidites or by exhumation of buried sulfide during channel flank erosion and slumping. Sulfidic conditions may be maintained by the mineralization of decomposition products from local benthic macrofauna or bacterial symbionts or by the production of more crystalline Fe(III) oxide phases that are less thermodynamically favorable than sulfate reduction in these bioturbated sediments. Overall, the iron and sulfur biogeochemical cycling in this environment is unique and much more similar to a coastal ecosystem than a deep-sea environment.

Please note that this is an author-produced PDF of an article accepted for publication following peer review. The definitive publisher-authenticated version is available on the publisher Web site.

Keywords : Sediment diagenesis, Iron reduction, Sulfate reduction, Deep-sea fans

Please note that this is an author-produced PDF of an article accepted for publication following peer review. The definitive publisher-authenticated version is available on the publisher Web site.

1.0 Introduction

Understanding the biogeochemical processes involved in the respiration of natural organic matter (NOM) in marine sediments is critical, as sediments represent the ultimate sink of carbon on Earth and the release of dissolved inorganic carbon (DIC) to the overlying waters, as by-product of respiration processes, may affect CO_2 inputs from the atmosphere to the oceans and, therefore, ocean acidification. Although aerobic respiration is the most efficient NOM degradation process (Hedges et al., 1995; Burdige, 2007), anaerobic processes are generally recognized to be significant in sediments exposed to high sedimentation rates. In these sediments, the high concentrations of NOM settled to the seafloor promotes consumption of the majority of the oxygen available by diffusion across the sediment-water interface (Burdige, 2006). These environments include estuaries (Martens et al., 1978; Aller and Yingst, 1980; Meiggs and Taillefert, 2011), coastal bays (Thamdrup et al., 1994), deltas (Aller et al., 1986; Pastor et al., 2011), and some continental margins dominated by large inputs of fine grained sediments from large rivers (Aller et al., 1986; McKee et al., 2004; Rabouille et al., 2009; Beckler et al., 2016). In these sediments, sulfate reduction is often the main anaerobic terminal electron accepting process (e.g. Jörgensen, 1982; Howarth, 1984; Hoehler et al., 2001) given the large concentrations of sulfate in seawater and the fact that one mole of sulfate is able to oxidize two moles of organic carbon all the way to DIC. Evidence, however, indicates that the reduction of Mn(IV/III) and Fe(III) oxides by metal-reducing bacteria may also contribute to a significant fraction of carbon remineralization processes in environments with significant inputs of minerals (Canfield et al., 1993; Lowe et al., 2000; Thamdrup and Canfield, 1996;

Kostka et al., 2002; Meiggs and Taillefert, 2011; Beckler et al., 2016), despite the fact that two moles of Mn(IV) and four moles of Mn(III) or Fe(III) are required to oxidize one mole of organic carbon. In these environments, the importance of metal oxides on carbon remineralization processes partly relies on their recycling upon exposure to oxygen (van der Zee et al., 2002; Wehrmann et al., 2014). As the abiotic oxidation of Fe^{2+} by dissolved oxygen is extremely fast at circumneutral pH (Sung and Morgan, 1980; Davison and Seed, 1983; Millero et al., 1987), a significant fraction of the oxygen consumption rate in sediments may be attributed to the recycling of Fe(III) oxides near the sediment-water interface. On the other hand, the abiotic oxidation of Mn^{2+} by dissolved oxygen is slow at circumneutral pH (Diem and Stumm, 1984; Davies and Morgan, 1989) and Mn^{2+}-oxidizing bacteria are required to facilitate the recycling of Mn(IV) oxides (Tebo et al., 2004).

Unfortunately, microbial reduction of Mn(IV/III) and Fe(III) oxides is difficult to demonstrate directly in the field, as unique molecular or genetic markers for these processes have yet to be identified (DiChristina et al., 2005). In addition, dissolved sulfide produced by sulfate reduction is a great reductant of both Mn(IV/III) (Burdige et al., 1985; Herzage and dos Santos Afonso, 1995) and Fe(III) oxides (dos Santos Afonso and Stumm, 1992; Peiffer et al., 1992). As these reactions simultaneously remove dissolved sulfide and generate Mn^{2+} and Fe^{2+} in pore waters, it is difficult to differentiate sulfide-driven reduction of these metal oxides from microbial metal reduction, especially in iron-rich sediments where a cryptic sulfur cycle may be responsible for the production of Fe^{2+} in the pore waters (Aller et al., 2010). Similarly, the precipitation of FeS in the presence of excess dissolved sulfide (Pyzik and Sommer, 1981; Rickard, 1995) and the eventual generation of

pyrite (Rickard and Luther, 1997) represent two additional processes that scavenge reduced iron and dissolved sulfides from the pore waters. The occurrence of these processes can be inferred from the solid phase, however, as FeS is a dense black precipitate. Chemical tracers of microbial iron reduction and precipitation of FeS were recently adopted to identify the zones of sulfate reduction in situ without the addition of radiotracers (Beckler et al., 2016). In this approach, organic-Fe(III) complexes detected by voltammetric mercury-gold amalgam (Hg/Au) microelectrodes below the oxygen penetration depth were used as proxy for microbial iron reduction, as these complexes are produced as intermediates during the reduction of Fe(III) oxides by several strains of the *Shewanella* genus (Taillefert et al., 2007; Jones et al., 2010). In addition, the existence of organic-Fe(III) complexes in oxygen-depleted pore waters indicates that sulfate reduction is not ongoing, as the reduction of these Fe(III) complexes by dissolved sulfide is extremely fast (Taillefert et al., 2000a). Simultaneously, $FeS_{(aq)}$ clusters detected by voltammetric Hg/Au microelectrodes may be used as proxy for the zone of sulfate reduction, as these clusters are intermediates in the precipitation of FeS (Theberge et al., 1997; Rickard et al., 1999; Taillefert et al., 2000a; Rickard, 2006).

In this paper, the coupling between iron and sulfur biogeochemistry in the sediments from the active lobe complex of the Congo River deep-sea fan is examined using both field measurements and theoretical model considerations. Sediments from the levees along the main channel of this deep-sea fan are compared to those off axis, including an old extinct channel. In addition, the sediment geochemistry is examined in discrete habitats colonized by micro- and megafauna along the main channel to determine the biogeochemical

116 conditions that lead to the existence of these unsual ecosystems.

117 2.0 Sampling and Methods

118 Sediment cores from the active lobe complex of the Congo River deep-sea fan were
119 obtained using either a multicorer or by the ROV Victor 6000 (Ifremer, Brest, France) from
120 5 stations approaching 5,000 m depth and up to 800 km offshore (Figure 1) during a cruise
121 on the N/O *Pourquoi Pas?* (Ifremer, Brest, France) from December 2011 to January 2012
122 (Rabouille, 2011). Stations were located along two perpendicular transects: one along-axis
123 extending from the entrance of the main channel to the main present deposition zone (Site
124 A, 4755-4769 m; Site F, 4861-4868 m; Site C, 4944-4967 m); and one off-axis from the
125 entrance of the canyon (Site A), to a station ~10 km north from the active channel (Site B,
126 4816-4823 m), and to an extinct channel no longer receiving turbidite flows (Site E, 4750
127 m). The multicorer was used to sample sediments from the levees along the active channel,
128 whereas the push cores were deployed from the ROV Victor 6000 around discrete habitats
129 that were either deeply reduced, populated by microbial mats, or colonized by
130 chemosynthetic megafauna, including species of *Vesicomyidae* bivalves (Table 1). More
131 details on the stations and the sampling locations along the Congo River deep-sea fan are
132 provided in the first paper of this special edition (Rabouille et al., this issue). Sediment
133 cores from the multicorer (7 cores) consisted of 9.6 cm ID x 70 cm long cores, whereas
134 push cores obtained by the ROV (10 cores) consisted of 6 cm ID x 50 cm long cores. Cores
135 were immediately processed after recovery by first measuring depth profiles of the main
136 redox species and pH in the intact cores at 4°C using voltammetric and potentiometric
137 microelectrodes. Pore waters were then extracted from the same cores under N_2

atmosphere in a glove bag and in a cold room to maintain in situ temperature (4°C). Sediment cores were sliced in sections of typically 7 mm and centrifuged under N_2 atmosphere at 3000 rpm for 10 minutes to extract pore waters. The supernatant was then collected with syringes under N_2 atmosphere, filtered through 0.2 μm PES Puradisc syringe filters (Whatman), and either stabilized in HCl 0.1 M, added to reagents for colorimetric detection (iron speciation and orthophosphate), preserved unacidified for immediate analysis (silicates, dissolved inorganic carbon, $\Sigma NO_x^- = NO_2^- + NO_3^-$), or frozen for analyses at a later date (sulfate, chloride, ammonium). The leftover sediments were stored at -20°C until the ship returned to port, then were shipped on dry ice to Georgia Tech for chemical extractions.

Depth profiles of the main redox species $O_{2(aq)}$, Fe^{2+}, Mn^{2+}, $\Sigma H_2S = (H_2S + HS^- + S^{(0)} + S_x^{2-})$, as well as $S_2O_3^{2-}$ (Brendel and Luther, 1995), organic-Fe(III) complexes (Taillefert et al., 2000a), and $FeS_{(aq)}$ clusters (Theberge and Luther, 1997) were detected by voltammetry with a single solid state mercury-gold (Hg/Au) voltammetric microelectrode encased in Pyrex glass with a tip diameter < 1 mm. The voltammetric microelectrode was lowered in the sediment cores maintained at 4°C with an ice bath via a computer-operated Analytical Instrument Systems, Inc. (AIS, Inc.) micromanipulator capable of submillimeter increments. The voltammetric microelectrode was used as part of a 3-electrode system consisting also of Ag/AgCl reference and Pt counter electrodes positioned in the overlying waters during the measurements. All voltammograms were obtained with a AIS, Inc. DLK-60 or DLK-100 potentiostat. Solid-state Hg/Au voltammetric microelectrodes and reference and Pt counter electrodes were constructed as previously reported (Brendel and

160 Luther, 1995; Luther et al. 2008). The mercury amalgam was plated on the gold surface of
161 the voltammetric microelectrode by maintaining the electrode at -0.1 V for 4 minutes in a
162 0.1 M $Hg(NO_3)_2$ solution in 0.05 M HNO_3 and stabilized by applying a potential of -9.0 V
163 at the Hg/Au microelectrode in a 1 M NaOH solution for 90 seconds (Brendel and Luther,
164 1995). The AgCl coating was formed on the reference electrode by applying +9V between
165 the Ag wire and a Pt electrode (Brendel and Luther, 1995).

166 Dissolved O_2 was detected by linear sweep voltammetry (LSV) using a scan rate of 200
167 mV/s between -0.1 V and -1.85 V to quantify both the current waves of $O_{2(aq)}$ and the H_2O_2
168 intermediate formed at the surface of the electrode. All other species were detected by
169 cathodic square wave voltammetry using a 200 mV/s scan rate between -0.1 V and -1.75 V
170 after a conditioning step at -0.1 V for 10 sec. to clean electrodes between measurements. If
171 organic-Fe(III) complexes or dissolved sulfides were detected an additional conditioning
172 step at -0.9 V for 10 s was added before each measurement to clean the electrodes
173 (Taillefert et al., 2000b; Luther et al., 2008; Tercier-Weber and Taillefert, 2008). If sulfide
174 concentrations were high, anodic square wave voltammetry between -1.75 V and -0.1 V at
175 a scan rate of 200 mV/s and without conditioning step was preferred to measure ΣH_2S, as it
176 minimizes the formation of HgS double films on the electrode surface (Davison et al.,
177 1988). As overlying waters were not fully oxygenated, Hg/Au voltammetric
178 microelectrodes were calibrated for $O_{2(aq)}$ externally in a 0.54 M NaCl solution equilibrated
179 with the atmosphere at 4^oC. Hg/Au voltammetric microelectrodes were then calibrated for
180 Mn^{2+} in a $MnCl_2$ solution (0 to 400 μM), and the pilot ion method (Brendel and Luther,
181 1995; Luther et al., 2008) was used to infer concentrations of Fe^{2+} and ΣH_2S in samples. As

182 the exact chemical composition of the organic-Fe(III) complexes and $FeS_{(aq)}$ are unknown,
183 their voltammetric responses are directly reported in current intensities (Taillefert et al.,
184 2000a). To compare the signal intensities of these species measured at different electrodes,
185 each electrode's response to Mn^{2+} was normalized to a typical Mn^{2+} response, and this ratio
186 was used to adjust the current response of the unquantifiable analytes. Peak heights were
187 determined using a semi-automated VOLTINT software package (Bristow and Taillefert,
188 2008). Depth profiles of pH were obtained within 2 cm of the voltammetric microelectrode
189 by lowering a 11 cm long double junction pH microelectrode of < 1 mm diameter
190 (Microelectrodes, Inc.) on the same micromanipulator and recording potentials with the
191 AIS, Inc. DLK potentiostat. The pH microelectrode was calibrated externally by recording
192 the potential and temperature of a TRIS buffer in artificial seawater (Dickson, 1993) before
193 and after deployments, and the Nernst equation was used to calculate the pH from potential
194 and temperature measurements (Skoog and Leary, 1996). Although pH values may be
195 affected by changes in the carbonate saturation state of the pore waters due to changes in
196 pressure upon recovery of the sediment, the relative pH changes with depth can still be
197 used to study the biogeochemical processes involved in these sediments.

198 Soluble orthophosphates (ΣPO_4^{3-}) were measured colorimetrically onboard the ship using
199 the molybdate-blue method (Murphy and Riley, 1962). Dissolved inorganic carbon (DIC)
200 was measured by flow-injection analysis (Hall and Aller, 1992) immediately after
201 sampling. The speciation of iron was also measured colorimetrically onboard the ship in
202 filtered samples by the ferrozine method (Stookey, 1967) after reduction with 0.2 M
203 hydroxylamine hydrochloride in HCl 0.1 M to quantify total dissolved Fe or without

reductant to quantify dissolved Fe^{2+}. The concentration of ΣNO_x^- (= NO_3^- + NO_2^-) was measured by flow-injection analysis after reduction with cadmium (Hale et al., 2004) onboard the ship, whereas ammonium was quantified spectrophotometrically (Strickland and Parsons, 1974) back at Georgia Tech. Finally, poorly crystalline and crystalline iron were determined in triplicate by ascorbate and dithionite extractions with ferrozine analysis (Kostka and Luther, 1994) at Georgia Tech. A select number of samples were also analyzed for acid volatile sulfide (AVS) by voltammetry after extractions with 0.3 M HCl according to previous methodologies (Henneke et al., 1991).

The saturation state of the pore waters with respect to mackinawite as a function of depth in each sediment core was calculated from the concentrations of total dissolved sulfide (ΣH_2S) and Fe^{2+} measured by voltammetry and the pH measured simultaneously by potentiometric microelectrode. The mackinawite solubility constant of log $K_{sp,2}$ = 3.5 (Rickard, 2006) was used for these calculations. The speciation of sulfide was calculated with an acid-base constant of pKa_1 = 6.88 (Millero, 1986), assuming ΣH_2S constituted only of H_2S and HS^-. Finally, the activity coefficients of H_2S and Fe^{2+} in seawater were calculated using Pitzer's equation (Beckler et al., 2016). The saturation index was reported as the logarithm of the ion activity product of the reaction over the solubility constant.

Diffusive oxygen uptake (DOU) fluxes and the maximum upward diffusive fluxes of Mn^{2+}, Fe^{2+}, ΣH_2S (assuming HS^- constituted the majority of ΣH_2S), dissolved inorganic carbon (DIC; assuming HCO_3^- constituted the majority of DIC), and NH_4^+ were calculated from the pore water data of each sediment core using Fick's first law according to a previous

method (Beckler et al., 2016). Molecular diffusion coefficients of the ions were corrected for temperature using empirical relationships (Boudreau, 1997), whereas that of dissolved oxygen was calculated at the pressure, salinity, and temperature of the in situ environment (Boudreau, 1997). The effect of tortuosity on diffusion coefficients was accounted for using Archie's law (Ullman and Aller, 1982), and concentrations were modified to account for the porosity of the sediment. Finally, the contribution of each anaerobic process to carbon remineralization was quantified assuming DOU fluxes represented the ultimate oxidant.

3.0 Results

3.1 Diagenetic processes in levee sediments

Sediments from the levees displayed similar depth profiles of the main redox constituents involved in the diagenesis of natural organic matter along the main channel from the bottom of the slope (Site A), to midway along the channel (Site F), and to the youngest lobe (Site C). The penetration depth of dissolved oxygen varied between 6 and 8 mm at Site A and Site C to around 14 mm at Site F, and these sediments were dominated by iron reduction as evidenced by the production of Fe^{2+} in the pore waters of each sediment core (Figure 2a-c). Reduced iron was produced within ca. 20 mm from the oxygen penetration depth in Site A sediments, in concentrations that reached up to 700 μM by 80 mm and remained constant deeper (Figure 2a). In contrast, Fe^{2+} was only produced in the pore waters below 80 mm at Site F and increased in two different gradients, a small one between 68 and 130 mm that reached about 100 μM Fe^{2+}, and a large gradient below 140 mm to reach as much as 650 μM at 165 mm depth (Figure 2b). Finally, reduced iron was produced

247 within 15 mm from the oxygen penetration depth at Site C to form a subsurface peak of 290
248 μM Fe^{2+} at 27 mm, then decreased below that depth to reach a concentration stabilizing
249 between 100 and 180 μM below 50 mm (Figure 2c). The production of Fe^{2+} was mirrored
250 by the production of organic-Fe(III) complexes at depth in the sediments of Site A, Site F,
251 and Site C with current intensities that generally decreased moving out from the bottom of
252 the slope (Site A) along the banks of the main channel (Site F) to the youngest lobe (Site C)
253 at the end of the fans (Figure 2a-c). Reduced manganese was only detected below 45 mm at
254 Site C in the levee sediments (Figure 2c) and increased asymptotically below that depth to
255 a maximum of 200 μM in the pore waters. Nitrate/nitrite ($\Sigma NO_x^- = [NO_3^-] + [NO_2^-]$)
256 decreased from about 25 μM in the overlying waters to below detection limit by 20 mm at
257 all three stations along the main channel (Figure 2a-c). Interestingly, a subsurface peak in
258 ΣNO_x^- was observed below the zone of denitrification in each of these three stations with
259 maxima of 110 μM 45 mm below the sediment-water interface at Site A (Figure 2a), 7 μM
260 at 45 mm at Site F (Figure 2b), and 55 μM at 35 mm at Site C (Figure 2c) that generally
261 coincided with the onset of Fe^{2+} in the pore waters. Although more research on the origin of
262 these ΣNO_x^- subsurface maxima is needed, their possible link to the onset of Fe^{2+}
263 production suggests that Fe(III)-coupled anaerobic nitrification (Huang and Jaffe, 2015)
264 may be ongoing in these sediments. Total dissolved sulfide and voltammetric signals for
265 aqueous clusters of FeS were never detected in any of the pore waters in the levee
266 sediments, suggesting that sulfate reduction was not established in levee near-surface
267 sediments along the main channel (Figure 2a-c). The pH behaved similarly in all levee
268 sediments along the main channel: At Site A, it decreased linearly from 8.1 in the overlying
269 waters to ca. 7.5 at 10 mm, then in another linear gradient to 7.3 at 60 mm, before

rebounding slightly to 7.4 below 160 mm (Figure 2a). At Site F and Site C, the pH decreased asymptotically from around 8.0 in the overlying waters to 7.35 at 55 mm at Site F (Figure 2b) and 7.2 at 40 mm at Site C (Figure 2b), then stabilized around these values deeper. Not surprisingly, the concentrations of total reactive iron oxides obtained by dithionite extraction were extremely high in the iron reduction-dominated levee sediments, reaching up to 600 μmol gdw^{-1} at Site A, 1000 μmol gdw^{-1} at Site F, and 1100 μmol gdw^{-1} at Site C (Figure 2a-c). More remarkable, was the observation that most of the total reactive iron oxide fraction was also extracted by ascorbate (82 +/- 18% at Site A, 67 +/-16% at Site F, and 78 +/- 18% at Site C), indicating that the iron mineral fraction of most of these sediments constituted of highly reactive poorly crystalline iron oxides such as ferrihydrite. Dissolved inorganic carbon (DIC) was produced in all the levee sediments and increased rather constantly from around 2 mM at the sediment-water interface to approximately 8 mM at 105 mm at Site A, 6 mM at 130 mm at Site C, and 13.5 mM at 135 mm at Site F (Figure 2a-c). Simultaneously, the depth profiles of NH_4^+ mirrored those of DIC and increased from a few micromolar below the maximum penetration depth of dissolved oxygen to a maximum of 300 μM at Site A and Site C (Figure 2a and c), and 480 μM at Site F (Figure 2b). Finally, soluble orthophosphate (ΣPO_4^{3-}) were generally low in the pore waters of the levee sediments but, as with DIC, increased rather constantly with depth from below detection limit at the sediment-water interface to 4 μM 120 mm below the sediment-water interface at Site A (Figure 2a), 30 μM at 115 mm at Site F (Figure 2b), and 6 μM at 115 mm at Site C (Figure 2c).

Diagenetic processes off axis from the active channel generally decreased in intensity from

292 the levees at Site A, to Site B located slightly off axis, and to Site E an old extinct channel
293 further north of the active channel. Although dissolved oxygen was completely consumed
294 in the off axis sediments, the oxygen penetration depth increased from ~ 8 mm at Site A
295 (Figure 2a), to ~13 mm at Site B (Figure 2d), and to more than 60 mm at Site E (Figure 2e),
296 indicating a decrease in respiration intensity. In addition, pore water Fe^{2+} concentrations
297 were much lower and organic-Fe(III) complexes were not detected in appreciable currents
298 in the top sediments (< 90 mm) at Site B even if iron reduction dominated respiration
299 processes in these sediments (Figure 2d). A small subsurface Fe^{2+} peak was found below
300 the oxygen penetration depth, but Fe^{2+} concentrations decreased below 20 mm to below
301 detection limit by 60 mm. Reduced iron reappeared at 90 mm, increased to a maximum of
302 220 μM Fe^{2+} at 120 mm, then stabilized until 165 mm concomitantly with organic-Fe(III)
303 complexes. Although organic-Fe(III) signals remained relatively constant deeper, Fe^{2+} was
304 abruptly removed from the pore waters at 165 mm and disappeared by 190 mm. In turn,
305 evidence for iron reduction was not found in the sediments of the extinct channel, as Fe^{2+}
306 was never detected in the pore waters and organic-Fe(III) currents were only produced in
307 low current intensities below 80 mm (Figure 2e). Although a subsurface peak in ΣNO_x^- was
308 found immediately below the sediment-water interface in Site B sediments (Figure 2d),
309 denitrification was complete by the oxygen penetration depth (~ 20 mm), and another
310 subsurface peak was found between 40 and 70 mm, as at the stations along the main
311 channel, though in much lower concentrations (ca. 7 μM). In contrast, ΣNO_x^-
312 concentrations only peaked immediately below the sediment-water interface in Site E
313 sediments and gradually decreased to below detection limit at 90 mm depth (Figure 2e). As
314 in the other sediments, the pH profiles of the two stations off axis from the main channel

315 decreased below the sediment-water interface with a gradient that mirrored the dissolved
316 oxygen profile. As metal reduction was not intense at both stations, the pH remained
317 constant throughout both sediments around 7.2 at Site B (Figure 2d) and around 7.8 at Site
318 E (Figure 2e). The lower reduction intensity at these two stations correlated with the
319 generally lower concentrations of total reactive iron oxides in the solid phase. Although
320 variable, concentrations of total reactive iron oxides obtained by the dithionite extraction at
321 Site B and Site E did generally not exceed 500 μmol g^{-1}, and the fraction of ferrihydrite was
322 relatively large (80 +/- 24% at Site B and 85 +/- 22% at Site E). In agreement with the
323 decrease in respiration intensities off axis from the main channel, DIC concentrations
324 gradually increased from around 2 mM below the sediment-water interface to a maximum
325 of 11 mM at Site B and 5 mM only at Site E (Figure 2d-e). Similarly, NH_4^+ concentrations
326 increased from a few micromolar below the oxygen penetration depth to 380 μM at Site B
327 and 100 μM Site E, whereas dissolved orthophosphate concentrations only reached 2 μM
328 at Site B and 8 μM at Site E.

329 **3.2 Diagenetic processes in the sediments along the active channel**

330 **3.2.1 *Vesicomyidae* habitats**

331 Habitats dominated by *Vesicomyidae* displayed extreme gradients within tens of
332 centimeters from the center of active habitats observed at Site A (Figure 3) and Site C
333 (Figure 4), as well as from a patch of dead organisms collected at Site B (not shown).
334 Outside these habitats (Figure 3c and Figure 4c), diagenetic processes remained intense as
335 dissolved oxygen was removed within 3 mm from the sediment-water interface at Site A
336 (Figure 3a), 4 mm at Site B (not shown), and 5 mm at Site C (Figure 4a) (see also Pozzato

et al., this issue for fine scale oxygen measurements). Anaerobic respiration processes were dominated by iron reduction just outside the active patches with Fe^{2+} concentrations reaching as much as 600 μM immediately under the oxygen penetration depth at Site A, oscillating between 450 and 600 μM within the first 2 cm from the sediment-water interface, before decreasing and stabilizing at 200 μM below 30 mm (Figure 3a). At Site C, Fe^{2+} was produced briefly along with Mn^{2+} between 5 and 10 mm and reappeared below 20 mm at concentrations oscillating around 200 μM (Figure 4a). Simultaneously, relatively small voltammetric signals for organic-Fe(III) were found below 10 mm at Site A, forming a peak of 30 nA at 23 mm, then decreasing and oscillating between 10 and 20 nA deeper (Figure 3a). In contrast, organic-Fe(III) complexes were produced simultaneously with Fe^{2+} and increased with depth to much higher current intensities at Site C (Figure 4a). Although $FeS_{(aq)}$ was not detected outside the *Vesicomyidae* habitat at Site A, ΣH_2S were detected in these sediments but remained below 5 μM across the entire profile (Figure 3a). In contrast, ΣH_2S were always below detection limit outside the patch at Site C, but relatively high voltammetric signals for $FeS_{(aq)}$ were detected throughout the profile, including a subsurface peak just above the onset of Fe^{2+} production (Figure 4a). Finally, the pH decreased concomitantly with dissolved oxygen, from 7.8 at 10 mm above the sediment surface to ca. 7.5 at the sediment-water interface at Site A (Figure 3a), suggesting aerobic respiration and Fe^{2+} oxidation were significant at the sediment-water interface, and remained constant below the sediment-water interface. The pH also appeared to mirror the dissolved oxygen profile at Site C but decreased to 6.8 around 5 mm, then rebounded deeper to reach up to 7.3 around 65 mm (Figure 4a). Outside the dead *Vesicomyidae* habitats observed at Site B, anaerobic respiration processes were much less intense, and

these sediments generally displayed high thiosulfate concentrations, low ΣH_2S concentrations, and absence of Fe^{2+} and organic-Fe(III) complexes (not shown).

The habitats dominated by active *Vesicomyidae* at Site A and Site C (Figure 3c and Figure 4c) were in turn characterized by two different redox regimes (Figure 3b and Figure 4b). First, the depth of oxygen penetration was less than 2 mm below the sediment-water interface in both patches, suggesting that respiration was extremely intense in these sediments. Only small concentrations of Fe^{2+} were recorded, and a moderate subsurface peak of organic-Fe(III) complexes was found within 40 mm from the sediment-water interface at Site A (Figure 3b), whereas a peak in Fe^{2+} and organic-Fe(III) complexes reaching ca. 250 μM and 280 nA were observed within the first 40 mm at Site C (Figure 4b). Although ΣH_2S were not detected over the first 40 mm at Site A and Site C, small $FeS_{(aq)}$ signals were formed over that distance at Site A (Figure 3b) suggesting sulfide was formed in that zone or diffused from below. At Site C, evidence for sulfate reduction was not detected above 40 mm (Figure 4b). Below 40 mm, the concentration of ΣH_2S increased up to 3500 μM between 50 and 70 mm at Site A, then decreased to around 2500 μM deeper, while voltammetric signals for $FeS_{(aq)}$ remained below detection (Figure 3b). At Site C, ΣH_2S were below detection limit until 140 mm, where small concentrations were observed (<10 μM), but small $FeS_{(aq)}$ signals were formed below 120 mm, indicating the presence of sulfate reduction (Figure 4b). The pH reflected the presence of these two redox zones. It gradually decreased from 7.6 at the sediment-water interface at Site A to 7.47 at 40 mm, then rebound deeper to 7.65 at 90 mm (Figure 3b). The pH sharply decreased from 7.9 in the overlying waters at Site C to 7.3 at 7 mm, remained constant until 40 mm, then

382 rebounded gradually to a maximum of 7.5 at 150 mm (Figure 4b). Solid FeS was only
383 quantified at Site A, where it increased below the sediment-water interface from around 30
384 to 100 μmol g^{-1} between 40 and 50 mm, then decreased drastically below that depth (Figure
385 3b). Finally, DIC, NH_4^+, and ΣPO_4^{3-} reflected the intensity of sulfate reduction in the
386 *Vesicomyidae* habitats at both Site A and Site C. They increased from 3 mM DIC, 250 μM
387 NH_4^+, and 50 μM ΣPO_4^{3-} at the sediment-water interface at Site A to a maximum of 15 mM
388 DIC, 2200 μM NH_4^+, and 100 μM ΣPO_4^{3-} at 56 mm, then decreased slightly below (Figure
389 3b). At Site C, DIC, NH_4^+, and ΣPO_4^{3-} increased from 3 mM, 26 μM, and 0.7 μM below the
390 sediment-water interface to 50 mM DIC, more than 6000 μM NH_4^+, and almost 800 μM
391 ΣPO_4^{3-} at 130 mm deep (Figure 4b), with a sharp break at 8 cm possibly linked to
392 bioirrigation by *Vesicomyidae*. These large concentration increases most probably reflect
393 the extremely high intensity of anaerobic respiration in the sediments of this established
394 *Vesicomyidae* habitat. In contrast, anaerobic respiration activity was limited in the patch of
395 dead *Vesicomyidae* at Site B, as indicated by the lack of iron reduction, the production of
396 dissolved sulfide detected only below 160 mm, and the presence of large concentrations of
397 thiosulfate (not shown).

398 **3.2.2 Reduced sediments and microbial mats**

399 Depth profiles of the main redox species involved in the respiration of NOM in reduced
400 sediments (Figure 5a) and microbial mats (Figure 6a) from Site C also displayed
401 sulfate-reducing conditions immediately below the sediment-water interface (Figure 5b
402 and Figure 6b). These two habitats, however, displayed some contrasting features that
403 merit to be highlighted. Whereas the maximum oxygen penetration depth in the reduced

404 sediment sampled was at the sediment-water interface (Figure 5b), that of the white
405 microbial mat was around 5 mm (Figure 6b). Simultaneously, the intensity of sulfate
406 reduction was so intense in the reduced sediment that around 3000 μM ΣH_2S was found
407 between 25 and 100 mm from the sediment-water interface and ΣH_2S even diffused across
408 the sediment-water interface (Figure 5b). In the white mat, however, only 500 μM ΣH_2S
409 was produced between 30 and 40 mm depth, and though ΣH_2S appeared to diffuse upward,
410 it disappeared by 13 mm depth and a small peak in thiosulfate, a product of sulfide
411 oxidation, reaching 180 μM was found between 4 and 13 mm (Figure 6b). The production
412 of ΣH_2S in both environments was also accompanied by the production of between 500 and
413 1500 μM Mn^{2+} (Figure 5b) and between 300 and 500 μM Mn^{2+} (Figure 6b) in the pore
414 waters of the reduced sediment and white mat, respectively. More importantly, $FeS_{(aq)}$
415 signals that mirrored the ΣH_2S profiles were found in both systems and reached some of the
416 highest current intensities ever recorded (e.g. Beckler et al., 2016; Brendel and Luther,
417 1995; Bull and Taillefert, 2001; Meiggs and Taillefert, 2011; Rickard et al., 1999;
418 Taillefert et al., 2000a; Taillefert et al., 2002; Tercier-Waeber and Taillefert, 2008) in the
419 reduced sediment (ca 220 nA, Figure 5b) and between 40 and 80 nA in the white mat
420 (Figure 6b). Simultaneously, the pH decreased from 8.05 at the sediment-water interface of
421 the reduced sediment to ca 7.75 at 11 mm and remained constant deeper in the sediments
422 (Figure 5b). It also decreased from 7.9 in the overlying waters to a minimum of 7.5 in the
423 suboxic zone of the white mat, then rebounded with the production of ΣH_2S to a maximum
424 of 7.65 (Figure 6b). Finally, solid phase FeS was also found in high concentrations in the
425 reduced sediment, and DIC, NH_4^+, and ΣPO_4^{3-} byproducts of the respiration of NOM
426 reached between 45 and 50 mM DIC, almost 4000 μM NH_4^+, and ca. 400 μM ΣPO_4^{3-}

(Figure 5b). These concentrations could not be determined in the white mats, as intact samples could not be collected.

4.0 Discussion

4.1 Microbial iron reduction in levee sediments

Sediments from the levees of the active lobe complex of the Congo River deep-sea fan are largely dominated by Fe reduction due to the large input of terrigenous material from the Congo canyon and the large proportion of reducible iron substrate present in this particulate material (Figure 2). As a result, levee sediments are characterized by low oxygen penetration depths (< 10 mm for Site A, Site B, and Site C and 15 mm for Site F) and relatively large concentrations of dissolved Fe^{2+} (Figure 2a-d) in contrast to an extinct channel (Site E) which displays large oxygen penetration depths (~70 mm) and no detectable dissolved Fe^{2+} in the pore waters (Figure 2e). Several lines of evidence indicate that microbial reduction is likely responsible for the formation of Fe^{2+} in levee sediments of the active channels. First, a good correlation is found between organic-Fe(III) and Fe^{2+} at all the sites (Figure 7), indicating that organic-Fe(III) complexes are formed concomitantly with Fe^{2+}. Electrochemical signals with Au/Hg voltammetric microelectrodes have demonstrated the presence of soluble Fe(III) complexed by organic ligands in suboxic marine sediments after collection (Brendel et al., 1995; Rickard et al., 1999; Taillefert et al., 2000a; Bull and Taillefert, 2001; Taillefert et al., 2002) and in situ using benthic landers (Tercier-Waeber and Taillefert, 2008; Meiggs and Taillefert, 2011; Beckler et al., 2016), demonstrating that the presence of these complexes does not result from artifacts during sampling. As these complexes react extremely rapidly with dissolved sulfides

449 (Taillefert et al., 2000a), their presence in significant current intensities in levee sediments
450 indicate either absence of dissolved sulfides in these sediments or higher rates of formation
451 of these complexes compared to consumption by dissolved sulfide. Although the
452 mechanism of formation of soluble organic-Fe(III) complexes in anaerobic sediments is
453 currently unknown, non-reductive dissolution of poorly crystalline Fe(III) oxides by
454 multidentate organic ligands may occur at circumneutral pH (Zinder et al., 1986; Bondietti
455 et al., 1993; Luther et al., 1996). Non-reductive dissolution of Fe(III) oxides, however,
456 cannot explain the simultaneous production of Fe^{2+} and organic-Fe(III) complexes in the
457 levees pore waters. These complexes are produced simultaneously with Fe^{2+} as
458 intermediate products in the bacterial reduction of iron oxides (Taillefert et al., 2007;
459 Fennessey et al., 2010; Jones et al., 2010). It was also recently proposed that
460 bacterially-produced Fe^{2+} may be chelated by dissolved organic matter and oxidized
461 abiotically by Fe(III) oxides to generate organic-Fe(III) complexes in coastal sediments
462 (Beckler et al., 2015). Regardless of the exact mechanism, bacterial involvement in the
463 simultaneous generation of Fe^{2+} and organic-Fe(III) complexes suggests that microbial iron
464 reduction represents a significant component of anaerobic respiration in levee sediments.
465 Second, poorly crystalline Fe(III) oxides likely represent the main source of Fe^{2+} in these
466 sediments, as they constitute between 80 and 100% of the total concentration of reactive
467 Fe(III) oxides available in these sediments (Figure 2). Poorly crystalline Fe(III) oxides are
468 highly bioavailable (Kostka et al., 1999; Roden, 2003), and thermodynamics predicts that
469 the energy available from these Fe(III) oxides is much more favorable than that from
470 sulfate reduction, despite the large concentration of sulfate in seawater (Beckler et al.,
471 2016). Third, dissolved sulfide (minimum detection limit < 0.2 μM) and $FeS_{(aq)}$ species

were never detected by voltammetric microelectrodes in any of the pore waters from levee sediments (Figure 2), sulfate concentrations remained constant around 28 mM in the pore waters (not shown), the sediments consisted of bright brown muds (not shown), typical of Fe(III) oxides-rich sediments, and AVS analyses confirmed that FeS was not formed in these sediments (not shown, minimum detection limit ~ 40 nmol g^{-1}). Finally, DIC concentrations essentially increased by a factor of 2 to 3 and sometimes 6 at depth in these sediments relative to the overlying waters (Figure 2), demonstrating anaerobic respiration is significant despite the absence of Mn^{2+} in most of the pore waters (Figure 2), relatively low nitrate concentrations typically found in the top 5 cm of the sediment (Figure 2), and lack of detectable sulfate reduction at least in the top 50 cm of these sediments. Evidence for microbial iron reduction in marine sediments is limited to environments with high deposits of Fe(III) oxides, namely sediments fed with materials from rivers. Estuarine sediments consist of the majority of these cases (Jones et al., 2011; Meiggs and Taillefert, 2011; Beckler et al., 2015), and deep-sea hydrothermal environments have been reported to contain unusual amounts of Fe(III) oxides that may sustain microbial iron reduction (Homoky et al., 2011). In turn, mounting evidence indicates that continental margin sediments exposed to inputs from large rivers may provide enough inorganic and organic material to sustain microbial iron reduction in deep-sea sediments (Aller et al., 1986; van der Zee et al., 2002; McKee et al., 2004; Beckler et al., 2016). The role of these environments on the carbon cycle has been largely ignored as sulfate reduction has always been considered the main anaerobic terminal electron accepting process (e.g. Lin and Morse, 1991) and only one electron from Fe(III) reduction is available to oxidize carbon. As Fe^{2+} is rapidly reoxidized by dissolved oxygen, the Fe(III) oxide could easily be

recycled near the sediment-water interface and maintain iron-reducing conditions in surficial sediments (van der Zee et al., 2002; Wehrmann et al., 2014) until enough reactive organic carbon is buried to promote sulfate reduction deeper in the sediment. At that point, dissolved sulfide could diffuse toward the sediment-water interface, permanently scavenge iron by forming sulfur minerals, and shifting the entire sediment column to sulfate-reducing conditions.

4.2 Discrete habitats dominated by dissimilatory sulfate reduction

Although the sediments of the lobe complex are mainly dominated by microbial iron reduction, numerous discrete habitats, including reduced sediments and sediments colonized by microbial mats and *Vesicomyidae*, exhibit large concentrations of dissolved sulfide (Figure 3, 5, and 6). Interestingly, these environments are mostly present along the flanks of the active channel (Sen et al., this issue). These sediments represent hot spots of sulfate reduction, as background sediments around these habitats exhibit contrasting pore water geochemistries with large concentrations of dissolved iron (e.g., Figure 3a and 4a) and sometimes mixtures of Fe^{2+} and tracers of sulfate reduction (i.e. $FeS_{(aq)}$ clusters), but no or little dissolved sulfide, especially in sediments at the edge of these discrete habitats (Figure 3a and 4a). From these contrasting geochemical observations and the sharp (i.e. not diffuse) boundaries of the habitats, we propose that the input of electron donor in the discrete habitats increases sulfate reduction rates and thus sulfide production rates in excess of microbial iron reduction rate in the Fe(III) oxide-dominated background. As a result, a titration process is triggered, in which FeS precipitates fast enough to consume most of the dissolved iron (Figure 8). The sharp boundary observed between the discrete

habitat and background thus represents the consequence of this active "titration" mechanism between iron and sulfide, with diffusion supporting dissolved components from both sides. These findings suggest that these hot spots of a couple of meters wide are either fueled by discrete reactive organic carbon material that promotes heterotrophic sulfate reduction and diffusion of dissolved sulfide or cold seeps of advected methane-rich fluids that promote anaerobic methane oxidation coupled to sulfate reduction (Caldwell et al., 2008). The concentration of NOM is high throughout the Congo River deep-sea fans (Rabouille et al., 2009; Baudin et al., 2010; Stetten et al., 2015) but also highly homogeneous as a function of depth (Baudin et al., 2010; Stetten et al., 2015). In addition, methane advection from a deep reservoir as in cold seeps has not been detected in these sediments (Rabouille et al., this issue), suggesting that discrete reactive organic carbon may be the source of these hot spots that allow sulfate reduction to be complete and methanogenesis to evolve (Pastor et al., this issue).

4.3 Metal reduction in sediments along the main channel

The concentration of total dissolved sulfide (ΣH_2S) can be represented versus dissolved Mn^{2+} (Figure 9a) and Fe^{2+} (Figure 9b) at depth in each of the sediments of the levees and the main channel at Site A, Site B, Site C, Site E, and Site F to determine whether the production of the reduced metals is driven by abiotic reduction of Mn(III/IV) (Burdige and Nealson, 1985; Herzage and dos Santos Afonso, 2003) and Fe(III) oxides (dos Santos Afonso and Stumm, 1992; Peiffer et al., 1992) by ΣH_2S. As ½ or one mole of reduced sulfur is required to reduce these metal oxides abiotically and form S(0) as by-product, any total dissolved sulfide concentration above the 1:1 line for Mn^{2+} (Figure 9a) and 1:2 line for

539 Fe^{2+} (Figure 9b) indicates excess sulfide is produced in these sediments and suggests the
540 production of reduced metal is controlled by abiotic reduction of their respective metal
541 oxides. Interestingly, the concentration of ΣH_2S in the pore waters of all the sediments
542 producing Mn^{2+} in solution is on (white mat at Site C) or above the 1:1 line (reduced
543 sediments at Site C and *Vesicomyidae* patch at Site A) (Figure 9a), demonstrating that the
544 production of Mn^{2+} in the pore waters along the main channel and its lobes is controlled by
545 the reduction of Mn(III/IV) oxides by the product of sulfate reduction. In turn, ΣH_2S was
546 not detected in any of the levee pore waters (Figure 2), and thus the ΣH_2S:Mn^{2+} couples all
547 fall below the 1:1 line in levee sediments (Figure 9a). Although these findings do not
548 provide proof of the lack of sulfide-driven reduction of Mn(III/IV) oxides, these data and
549 the fact that the solubility of MnS is too high (Engler and Patrick, 1975) to remove any
550 significant sulfides or reduced manganese from the pore waters suggest that Mn^{2+} could be
551 produced microbially in the levee sediments. Similarly, the concentrations of ΣH_2S and
552 Fe^{2+} at each depth in the sediments of the discrete habitats along the main channel and the
553 lobes also always fall above the 1:2 lines, except for one depth at Site F, suggesting that
554 most of the Fe^{2+} produced in the pore waters near the discrete habitats is of abiotic origin.
555 These data suggest that the precipitation of $FeS_{(s)}$ was also a sink for iron and sulfur in these
556 sediments, as also indicated by the generally black sediments found at these stations and
557 the presence of high FeS concentrations in the solid phase (Figure 3b and 5b). Indeed,
558 equilibrium calculations where sulfide and Fe^{2+} were detected simultaneously indicate that
559 these sediments were supersaturated with respect to mackinawite (Table 2). In addition, the
560 presence of molecular clusters of FeS in regions of little or no dissolved sulfide (Figure 3b
561 and Figure 4a and b) or high dissolved sulfides but no Fe^{2+} (Figure 5b and Figure 6b)

provides evidence for active precipitation of $FeS_{(s)}$ (Taillefert et al., 2000a) or dissolution of $FeS_{(s)}$ as the solid phase equilibrates with the pore waters (Rickard, 2006). Interestingly, the pore waters inside the patches were much more oversaturated than those at the periphery of the patches (Figure 3, Table 2), reflecting the lower concentrations of dissolved sulfides immediately surrounding the reduced patches of sediment. Finally, the pH also provides further evidence of $FeS_{(s)}$ precipitation in the pore waters, as most pH profiles in the sediments of the discrete habitats either remained low and constant around pH 7.4-7.6 (Figure 3a and 5b), or slightly increased to around these values at depth (Figure 3b, 6b, 4a, and 4b), the range of pH where the solubility of mackinawite is the lowest (Rickard, 2006). In contrast, ΣH_2S was never observed in the pore waters of the sediments from the levees, and the ΣH_2S and Fe^{2+} pore water concentrations all lay below the 1:2 line (Figure 9b), as was shown with Mn^{2+} (Figure 9a).

4.4 Role of benthic megafauna in iron and sulfur cycle

Simultaneously, the sediments from all the habitats populated by chemosynthetic-based benthic megafauna at Site A (Figure 3c) or Site C (Figure 4c) as well as some sediments populated by microbial mats at Site C (Figure 6) showed evidence for a zone of oxidation, typically in the first 40 mm from the sediment-water interface for habitats populated by *Vesicomyidae* (Figure 3b and Figure 4b) or within 10-15 mm from the sediment-water interface for habitats populated by white microbial mats (Figure 6b). These zones displayed either limited Fe^{2+} concentrations (< 300 μM) and voltammetric signals for organic-Fe(III) complexes (Figure 3b and Figure 4b) or sometimes thiosulfate in significant concentrations (e.g. Figure 6b), all indicative of the oxidation of dissolved

584 sulfide or eventually pyrite if dissolved Fe(III) is able to accumulate, or a lack of build-up
585 of dissolved sulfide, which allow iron-reducing conditions to develop. These zones were
586 typically underlined by sharp gradients in dissolved sulfide concentrations (Figure 3b and
587 Figure 6b), suggesting that sulfide oxidation by the *Vesicomyidae* symbiont (Dupperon et
588 al., 2013; Decker et al., this issue) or *Beggiatoa*-like microbial mats (Sassen et al., 1993;
589 Sen et al., this issue) is able to maintain suboxic conditions in the top few centimeters of
590 these habitats. These findings suggest that these habitats are colonized by
591 chemosynthetic-based benthic megafauna and microbial mats as a result of the existence of
592 a source of reduced sulfur at depth. Although the localized source of electron donor for
593 sulfate reduction has yet to be identified, anaerobic oxidation of methane (AOM) coupled
594 to sulfate reduction appears to be involved below ~10 cm, as anaerobic methanotrophs
595 (ANMEs) and methane (< 400 µM) have both been found at each of these discrete habitats
596 and isotopic evidence indicates it is of microbial origin (Pastor et al., this issue). Two main
597 processes may therefore explain the origin of these discrete habitats: First, these habitats
598 may be fed by a discrete source of labile natural organic matter that allows diagenetic
599 processes to proceed all the way to methanogenesis. This labile natural organic matter may
600 be directly brought from the Congo river (Baudin et al., 2010; Stetten et al., 2015; Baudin
601 et al., this issue) via turbidity currents. Alternately, the presence of exhumed reduced
602 sediments containing either dissolved sulfide or iron sulfide minerals on the flanks of the
603 channels where mass wasting under the form of slumps or debrites was demonstrated
604 (Dennielou et al., this issue) may explain the colonization of discrete habitats near the
605 channel flanks. In this context, sulfate reduction is the main anaerobic respiration process,
606 iron is reduced abiotically and immobilized in the solid phase, and benthic megafauna

607 colonizes these patches of reduced sediments that generate sulfide for their symbionts.
608 Two additional processes may maintain these habitats once colonized by *Vesicomyidae*.
609 First, labile organic matter from the degradation of dead benthic megafauna or their
610 bacterial symbiont may activate sulfate reduction for their survival (Levesque et al., 2005).
611 Second, the active bioturbation of the top 40 mm by the megafauna may reoxidize Fe^{2+} to
612 more crystalline Fe(III) oxide phases, such as goethite, which are less thermodynamically
613 favorable than sulfate reduction in deep-sea environments (Beckler et al., 2016). The
614 patchy distribution of chemosynthetic-based benthic megafauna in the levee sediments
615 (Sen et al., this issue) may preserve Fe(III) oxides under the form of poorly crystalline
616 material which may also explain why iron reduction conditions are sustained in levee
617 sediments. Regardless of the process, sulfate reduction is either complete or almost
618 complete (~2-10 mM sulfate at depth) in the discrete habitats (Pastor et al., this issue) such
619 that methanogenesis is allowed to develop in the deep sediments. These hypotheses should
620 be investigated, as evidence for such ecological coupling is scarce in the literature (Olu et
621 al., this issue).

622 **4.5 Role of Congo River deep-sea fan in carbon mineralization**

623 C:N ratios calculated from regressions between DIC and NH_4^+ concentrations as a function
624 of depth corrected for their diffusion coefficients in each sediment core collected (Table 3)
625 reveal generally low values at Site A, the station located at the entrance of the active lobe
626 complex, compared to most of the cores collected on the levees at Site F and Site C, the
627 channel stations the farthest from the slope. These findings suggest that natural organic
628 matter reaching the sea floor at Site A is enriched in nitrogen compared to the material that

629 travels far from the slope. Solid phase analyses, however, reveal a high homogeneity in the
630 composition of NOM across the levees (Baudin et al., 2010; Stetten et al., 2015; Baudin et
631 al., this issue), with C:N ratios from the solid phase ranging between 15 and 18 at Site A, 14
632 and 18.5 at Site F, and 14 and 16 at Site C (Stetten et al., 2015). These findings suggest that
633 the lower C:N ratios obtained from DIC and NH_4^+ in the pore waters at Site A are in fact
634 due to the precipitation of carbonates, such as siderite, in the solid phase. Diffusive fluxes
635 calculated for dissolved oxygen, ΣNO_x^- (assuming nitrate represented the majority of
636 ΣNO_x^-), and the reduced metabolites Mn^{2+}, $Fe^{2+,}$ and ΣH_2S (Table 3) were used to estimate
637 the fraction of carbon that is remineralized by denitrification (assuming dissimilatory
638 nitrate reduction to ammonium is not significant), as well as dissimilatory Mn(IV), Fe(III),
639 and sulfate reduction in all sediments collected (Figure 10). The diffusive oxygen uptake
640 (DOU) flux estimates for the levees are in good agreement with the DOU fluxes measured
641 with oxygen microelectrodes (1-3 mmol m^{-2} d^{-1}; Pozzato et al., this issue). Denitrification
642 of the subsurface maxima in ΣNO_x^- observed in the levee sediments was not considered in
643 these calculations, as these peaks represent the net difference between production and
644 consumption at these depths. Denitrification was therefore considered in the top 2 cm at
645 Site A, Site B, Site C, and Site F, and in the top 8 cm at Site E (Figure 2). Although these
646 calculations may provide conservative estimates of carbon remineralization processes, as
647 the abiotic reduction of Mn(IV) and Fe(III) oxides by dissolved sulfides, precipitation of
648 sulfur, iron, and manganese minerals, and adsorption of Mn(II) and Fe(II) onto the
649 sediment apparently decrease the contribution of anaerobic respiration processes to carbon
650 remineralization (Wenzhofer et al., 2002; Meiggs and Taillefert, 2011), the burial of these
651 elements in the solid phase equally affects total carbon remineralization rates calculated

652 from DOU fluxes. As a result, the relative contribution of each anaerobic respiration
653 process to total carbon remineralization should be accurate in sediments where sulfate
654 reduction is not significant and slightly underestimated in sediments where sulfate
655 reduction titrates Mn(IV) and Fe(III) oxides. No evidence of dissimilatory sulfate
656 reduction was found in any of the levee sediments, despite their high carbon content
657 (Baudin et al., 2010; Stetten et al., 2015). Similarly, dissimilatory manganese reduction did
658 not contribute to a significant fraction of total carbon remineralization, whereas
659 denitrification contributed to 4-12% of total carbon remineralization in the levee
660 sediments. On the other hand, dissimilatory iron reduction accounted for 10 to 25% of
661 carbon remineralization processes at Site F and Site C, where the most recent deposits are
662 found (Rabouille et al., this issue), and only between 2 and 6% at Site A, at the entrance of
663 the active lobe complex, where the coarser inorganic material is separated from the finer
664 fractions (Babonneau et al., 2002). These findings corroborate the hypothesis that a large
665 fraction of Fe^{2+} precipitates as carbonate minerals at Site A, suggest that these estimates are
666 conservatives, and reflect the idea that the high surface area of small Fe(III) oxide particles
667 at Site C and Site F increases the bioavailability of Fe(III) oxides (Roden et al., 2003;
668 Taillefert et al., 2007). Finally, the contribution of dissimilatory iron reduction to carbon
669 remineralization tended to decrease going off axis from the active channel from Site A, to
670 Site B, and to Site E where it did not contribute at all to carbon remineralization processes
671 (Figure 10a), despite the relatively low C:N ratio found at the site. In addition, the pore
672 water C:N ratios at Site B and Site E (Table 3) mirrored those of the solid phase (Stetten et
673 al., 2015), indicating little precipitation of Fe^{2+} carbonate mineral phases. Site E is
674 disconnected from the active canyon and, therefore, receives limited amounts of

675 terrigeneous organic matter and Fe(III) oxides. These findings suggest that the supply of
676 Fe(III) oxides may limit anaerobic respiration processes, but not the intensity of
677 respiration. Indeed, iron fluxes (McManus et al., 1997; van der Zee et al., 2002; Law et al.,
678 2009) and the contribution of iron reduction to carbon remineralization rates (Thamdrup
679 and Canfield, 1996; Esh et al., 2013) were much lower in other continental slope
680 sediments, though similar iron fluxes were determined in slope sediments fed by large
681 rivers (Severmann et al., 2010; Beckler et al., 2016) or in oxygen minimum zones exposed
682 to strong upwelling (Noffke et al., 2012). In contrast, sediments from the discrete habitats
683 displayed a generally much lower C:N ratio compared to the levee sediments, and carbon
684 remineralization processes were much more active, as displayed by the high diffusive
685 fluxes of DIC and NH_4^+ relative to the levee sediments (Table 3). Indeed, dissimilatory
686 sulfate reduction was extremely intense in these sediments with dissolved sulfide
687 concentrations (Barry et al., 1997; Levin et al., 2003; Fisher et al., 2012; Ristova et al.,
688 2012) or diffusive fluxes (Fisher et al., 2012; Ristova et al., 2012) resembling those
689 measured in cold seep environments populated by *Vesicomyidae*. Although the DOU
690 fluxes obtained in the discrete habitats (5-12 mmol m^{-2} d^{-1}, Table 3) were generally lower
691 that those obtained with oxygen microelectrodes (8-40 mmol m^{-2} d^{-1}, Pozzato et al., this
692 issue), likely due to the poor spatial resolution of the voltammetric microelectrodes in such
693 large gradients in dissolved oxygen, the sulfate reduction fluxes used to estimate the
694 percent carbon remineralized anaerobically (Figure 10) exceeded both the DOU fluxes and
695 the DIC fluxes (Table 3). As reduction of Mn(IV) and Fe(III) oxides by dissolved sulfide,
696 precipitation of FeS, and possibly pyrite remove reduced sulfur from the pore waters, it is
697 difficult to quantify exactly the contribution of dissimilatory sulfate reduction from these

698 data, but sulfate was either depleted or almost completely depleted (~2-10 mM sulfate at
699 depth) from the pore waters in the same habitats (Pastor et al., this issue), suggesting that
700 dissimilatory sulfate reduction was the most significant anaerobic respiration process in the
701 discrete habitats. These findings imply that the large Mn^{2+} flux observed (Table 3) was due
702 to abiotic reduction of Mn(IV) oxides by dissolved sulfides whereas the generally small
703 Fe^{2+} fluxes in the discrete habitats (Table 3) resulted from the precipitation of FeS and/or
704 pyrite.

705 **4.6 Evolution of these discrete habitats along the main channel**

706 Although the exact source of electron donor that leads to the high intensity of dissimilatory
707 sulfate reduction in the discrete habitats remains to be elucidated, it is possible to anticipate
708 the evolution of these habitats over time (Olu et al., this issue). The background sediment is
709 iron-rich and consists mainly of poorly crystalline Fe(III) oxides that are much more
710 thermodynamically favorable electron acceptors than sulfate over a wide range of
711 geochemical conditions (Beckler et al., 2016). The occurrence of chemosynthetic-based
712 benthic megafauna along the main active channel flanks is likely due to the presence of
713 dissolved sulfides in the surficial sediments that must either result from (i) the availability
714 of a labile source of organic matter that feeds heterotrophic microorganisms and leads to
715 sulfate-reducing conditions or (ii) the exhumation of dissolved sulfide or reduced sulfide
716 minerals by mass wasting (Dennielou et al., this issue; Sen et al., this issue). The
717 pre-existence of sulfide-oxidizing microbial mats may facilitate the recruitment of
718 *Vesicomyidae* by consuming the excess sulfide in the surface sediments (Guillon et al.,
719 2017; Olu et al., this issue). In that respect the reduced black sediment found at Site C

720 (Figure 5a) may be too reduced for *Vesicomyidae* colonization, as sulfate reduction is
721 intense and excessive concentrations of dissolved sulfides is toxic for these organisms
722 (Goffredi and Barry, 2002; Levin et al., 2003; Heyl et al., 2007) are detected all the way to
723 the surface of the sediment. The white microbial mats, on the other hand, may be more
724 suited to *Vesicomyidae*, as the sediment underlying the mats is partially oxidized and the
725 concentrations of dissolved sulfides are much lower than in the reduced sediment (Figure 5
726 and Figure 6). Such mat-dominated sediments may therefore represent intermediate stages
727 between the iron-reducing dominating conditions in the background sediment and the
728 highly reduced sediment. Once sulfate-reducing conditions are established, *Vesicomyidae*
729 colonization is possible and the surface sediment is slowly reoxidized via bioturbation to
730 bring dissolved oxygen to the sulfide front. As a result, the first 40 mm of sediment were
731 enriched in Fe^{2+} and/or organic-Fe(III) complexes (Figure 3b and Figure 4b), likely
732 produced by oxygenation of Fe^{2+} in the presence of organic ligands (Taillefert et al., 2000a)
733 and microbial iron reduction below the oxygen penetration depth (Beckler et al., 2015). In
734 these ecosystems, a range of sulfide flux was found that likely reflects their different
735 recruitment stages: high sulfide flux for PL484-CT10 at Site A (Table 3), suggesting young
736 *Vesicomyidae* habitat (Figure 3c); low sulfide flux for PL491-CT7 at Site C (Table 3),
737 measured on the edge of a mature *Vesicomyidae* habitat (Table 1) where active
738 precipitation of FeS with background dissolved Fe^{2+} likely decreased the flux of sulfide
739 (Figure 4c); and low to medium sulfide flux for PL494-CT3 at Site B (Table 3), suggesting
740 extinct or decaying *Vesicomyidae* habitat (not shown). The balance between
741 symbiont-based sulfide oxidation and sulfate reduction in the habitats populated by
742 *Vesicomyidae* does likely not last forever, either because the electron donor source that

743 fuels sulfate reduction eventually runs out or the sulfide requirements by the symbiont
744 exceed the supply of dissolved sulfide diffusing from the deeper sediment layers. In the
745 end, the life cycle of *Vesicomyidae* is reached and the sediment is slowly reoxidized back
746 to iron-reducing conditions from the top down, as recycling of Fe(III) oxides by dissolved
747 oxygen near the surface promotes oxidation of dissolved sulfides diffusing upward from
748 the deep sediment, while oxidation of FeS buried in the solid phase by dissolved oxygen
749 and possibly organic-Fe(III) complexes produced near the sediment-water interface may
750 slowly increase the redox state of the *Vesicomyidae* habitats. In these conditions, dissolved
751 sulfide has completely disappeared from the habitat, the oxygen and sulfide fluxes are
752 some of the lowest (Table 3), and the organisms do not survive, as for PL492-CT10 at Site
753 B (not shown). The eventual impact of these discrete habitats on the carbon, sulfur, and
754 iron cycle remain unknown, but their biogeochemistry and evolution over time appear to
755 resemble those of hydrothermal or cold seep environments, suggesting they may act as
756 important electron shuttle (i.e. transferring electrons from oxidized to reduced sulfur and
757 back to oxidized sulfur species) for a variety of ecologically relevant deep-sea
758 invertebrates.

759 5.0 Conclusions

760 In this study, the main biogeochemical processes regulating the remineralization of natural
761 organic matter were investigated in the sediments from the Congo deep-sea fan, a unique
762 environment located at the bottom of the continental slope of West Africa that is fed
763 tremendous amounts of inorganic and organic material from the Congo River. The
764 sediments from the levees along the main active channel of the fan demonstrated active

765 benthic respiration, with oxygen penetration depths between 6 and 8 mm. Anaerobic
766 respiration processes in the sediments were dominated by dissimilatory iron reduction,
767 likely because the majority of the Fe(III) oxides phases found in these sediments consisted
768 of poorly crystalline Fe(III) oxides which are thermodynamically more favorable than
769 sulfate reduction over a wide range of geochemical conditions. Although iron reduction
770 also dominated biogeochemical processes in the sediments of the main channel from the
771 entrance of the lobe complex to the most recent lobe of this deep-sea fan, distinct habitats
772 were discovered that were characterized by extremely low oxygen penetration depth (1-3
773 mm), large $FeS_{(s)}$-containing black precipitates, and dominated by dissimilatory sulfate
774 reduction. These habitats were either deeply reduced or populated by large communities of
775 *Vesicomyidae* bivalves that are known to contain sulfide-oxidizing symbionts or microbial
776 mats that remain to be identified. The colonized habitats dominated by *Vesicomyidae*
777 displayed generally a suboxic zone of 40 mm in which Fe^{2+} and organic-Fe(III) complexes
778 were found, suggesting the sulfide-oxidizing symbiont modified the geochemical
779 conditions of the underlying sediment. These habitats also displayed variable dissolved
780 sulfide fluxes and concentrations that seemed to reflect their different life stages. The
781 reduced black sediments revealed intense sulfate-reducing conditions that generated
782 dissolved sulfides all the way to the surface of the sediment. These ecosystems appeared to
783 be too reduced to promote colonization by the bivalves, suggesting they may represent a
784 primitive form of the habitats, before bivalve colonization. The white microbial mats
785 discovered also showed a small suboxic zone and were characterized by lower dissolved
786 sulfide concentrations and fluxes that may represent an intermediate state between the
787 iron-reduction dominated background sediment and the deeply reduced sediment. Finally,

788 the sediment mainly occupied by dead *Vesicomyidae* did not display any evidence of
789 sulfate reduction in the first 150 mm, except for the black color of the sediment, suggesting
790 that once sulfate reduction is exhausted, the habitats are drawn to extinction. The
791 biogeochemical reason for the presence of these highly reduced habitats is not clear. They
792 could be either produced by discrete inputs of labile natural organic matter from the Congo
793 River delivered by turbidites or by exhumation of reduced sulfides during mass wasting of
794 the channel flanks. *Vesicomyidae* colonies may also maintain themselves by generating
795 labile organic matter during their decomposition or the degradation of their bacterial
796 symbiont to fuel sulfate reduction. Alternately, bioturbation by the active megafauna may
797 be able to recycle Fe(III) oxides under the form of more crystalline phases that are less
798 thermodynamically favorable than sulfate reduction and thus jump start dissimilatory
799 sulfate reduction. Regardless of the sulfide-producing process, the existence of a clear
800 redox biogeochemical boundary between the discrete habitats and the background
801 sediment is attributed to the "chemical titration" of Fe^{2+} and HS^- which is mutually
802 exclusive once the production rate of one of them, i.e. iron in the background or sulfide in
803 the habitat, is larger. These hypotheses should be investigated further.

804 ## 6.0 Acknowledgments

805 We would like to acknowledge the captain and crew of the N/O Pourquoi Pas? and the
806 pilots and crew of the ROV Victor 6000 for their hard work during the cruise. We would
807 also like to thank Philippe Noel and Bruno Blombed for handling the multicorer, Francoise
808 Lesongeur for managing the push core collection, as well as the entire science crew of
809 Congolobe. This work was supported by the National Science Foundation [grant number

OCE-851156, OCE-1438648] and the Agence Nationale de la Research [grant number ANR Blanc SIMI5-6, n°11 BS56 030].

7.0 References

Aller, R.C., Yingst, J.Y., 1980. Relationship between microbial distributions and the anaerobic decomposition of organic matter in surface sediments of Long Island Sound, USA. Mar. Biol. 56, 29-42.

Aller, R.C., Mackin, J.E., Cox Jr., R.T., 1986. Diagenesis of Fe and S in Amazon inner shelf muds: apparent dominance of Fe reduction and implications for the genesis of ironstones. Cont. Shelf Res. 6, 263-289.

Aller, R.C., 1996. Mobile deltaic and continental shelf muds as suboxic, fluidized bed reactors. Mar. Chem. 61, 143-155.

Aller, R.C., Madrid, V., Chistoserdov, A., Aller, J.Y., Heilbrun, C., 2010. Unsteady diagenetic processes and sulfur biogeochemistry in tropical deltaic muds: Implications for oceanic isotope cycles and the sedimentary record. Geochim. Cosmochim. Acta 74, 4671-4692.

Babonneau, N., Savoye, B., Cremer, M., Klein, B., 2002. Morphology and architecture of the present canyon and channel system of the Zaire deep-sea fan. Mar. Pet. Geol. 19, 445-467.

Barry, J.P., Kochevar, R.E., Baxter, C.H., 1997. The influence of pore-water chemistry and physiology on the distribution of vesicomyid clams at cold seeps in Monterey Bay:

Implications for patterns of chemosynthetic community organization. Limnol. Oceanogr. 42, 318-328.

Baudin, F., Disnar, J.R., Martinez, P., Dennielou, B., 2010. Distribution of the organic matter in the channel-levees systems of the Congo mud-rich deep-sea fan (West Africa). Implication for deep offshore petroleum source rocks and global carbon cycle. Mar. Pet. Geol. 27, 995-1010.

Baudin, F., Stetten, E., Schnyder, J., Charlier, K., Martinez, P., Dennielou, B., Droz, L., 2016. Origin and distribution of the organic matter in the distal lobe of the Congo deep-sea fan – A Rock- Eval survey. Deep Sea Res. II. This issue.

Beckler, J.S., Jones, M.E., Taillefert, M., 2015. The origin, composition, and reactivity of dissolved iron(III) complexes in coastal organic- and iron-rich sediments. Geochim. Cosmochim. Acta 152, 72-88.

Beckler, J.S., Kiriazis, N., Stewart, F.J., Rabouille, C., Taillefert, M., 2016. Importance of microbial iron reduction in deep sediments of river-dominated continental margins. Mar. Chem. 178, 22-34.

Bondietti, G., Sinniger, J., Stumm, W., 1993. The reactivity of Fe(III) (hydr)oxides: effects of ligands in inhibiting the dissolution. Coll. Surf. A. 79, 157-174.

Boudreau, B.P., 1997. Diagenetic models and their implementation: modelling transport and reactions in aquatic sediments. Springer-Verlag.

849 Brendel, P.J., Luther III, G.W., 1995. Development of a gold amalgam voltammetric
850 microelectrode for the determination of dissolved Fe, Mn, O2, and S(-II) in pore waters
851 of marine and freshwater sediments. Environ. Sci. Technol. 29, 751-761.

852 Bull, D.C., Taillefert, M., 2001. Seasonal and topographic variations in porewaters of a
853 southeastern USA salt marsh as revealed by voltammetric profiling. Geochem. Trans.
854 13, 1-8.

855 Bristow, G., Taillefert, M., 2008. A Matlab-based program for semi-automated processing
856 of geochemical data acquired by voltammetry. Comput. Geosci. 34, 153-162.

857 Burdige, D.J., Nealson, K.H., 1985. Chemical and microbiological studies of
858 sulfide-mediated manganese reduction. Geomicrobiol. J. 4, 361-387.

859 Burdige, D.J., 2006. Geochemistry of marine sediments. Princeton University Press,
860 Princeton, New Jersey.

861 Burdige, D.J., 2007. Preservation of organic matter in marine sediments: Controls,
862 mechanisms, and an imbalance in sediment organic carbon budgets? Chem. Rev. 107,
863 467-485.

864 Caldwell, S.L., Laidler, J.R., Brewer, E.A., Eberly, J.O., Sandborgh, S.C., Colwell, F.S.,
865 2008. Anaerobic oxidation of methane: Mechanisms, bioenergetics, and the ecology of
866 associated microorganisms. Environ. Sci. Technol. 42, 6791-6799.

867 Canfield, D.E., Jorgensen, B.B., Fossing, H., Glud, R., Gundersen, J., Ramsing, N.B.,
868 Thamdrup, B., Hansen, J.W., Nielsen, L.P., Hall, P.O.J., 1993. Pathways of organic
869 carbon oxidation in three continental margin sediments. Mar. Geol. 113, 27-40.

870 Davies, S.H.R., Morgan, J.J., 1989. Manganese(II) oxidation kinetics on metal oxide
871 surfaces. J. Coll. Inter. Sci. 129, 63-77.

872 Davison, W., Seed, G., 1983. The kinetics of the oxidation of ferrous iron in synthetic and
873 natural waters. Geochim. Cosmochim. Acta 47, 67-79.

874 Davison, W., Buffle, J., De Vitre, R., 1988. Direct polarographic determination of O2,
875 Fe(II), Mn(II), S(-II), and related species in anoxic waters. Pure Appl. Chem. 60,
876 1535-1543.

877 Decker, C., Zorn, N., Le Bruchec, J., Caprais, J.-C., Potier, N., Leize-Wagner, E., Lallier,
878 F.H., Olu, K., Andersen, A.C., 2017. Can hemoglobin characteristics of vesicomyid
879 clam species influence their distribution in deep-sea sulfide-rich sediments? A case
880 study in the Gulf of Guinea. Deep Sea Res. II. This issue.

881 Dennielou, B., Droz, L., Jacq, C., Babonneau, N., Bonnel, C., Picot, M., Le Saout, M.,
882 Saout, Y., Bez, M., Savoye, B., Olu, K., Rabouille, C., 2017. Morphology, structure,
883 composition and build-up processes of the active Congo channel-mouth lobe complex
884 with inputs from remotely operated underwater vehicle (ROV) multibeam and video
885 surveys. Deep Sea Res. II. This issue.

886 DiChristina, T.J., Frederickson, J.K., Zachara, J.M., 2005. Enzymology of electron
887 transport: Energy generation with geochemical consequences. Rev. Mineral. Geochem.
888 59, 27-52.

889 Dickson, A.G., 1993. pH buffers for seawater media based on the total hydrogen ion
890 concentration scale. Deep-Sea Res. I 40, 107-118.

891 Dos Santos Afonso, M., Stumm, W., 1992. Reductive dissolution of iron(III) (hydr)oxides
892 by hydrogen sulfide. Langmuir 8, 1671-1675.

893 Dupperon, S., Gaudron, S.M., Rodrigues, C.F., Cunha, M.R., Decker, C., Olu, K., 2013.
894 An overview of chemosynthetic symbioses in bivalves from the North Atlantic and
895 Mediterranean Sea. Biogeosci. 10, 3241-3267.

896 Esch, M.E.S., Shull, D.H., Devol, A.H., Moran, S.B., 2013. Regional patterns of
897 bioturbation and iron and manganese reduction in the sediments of the southeastern
898 Bering Sea. Deep Sea Res. II 94, 80-94.

899 Fennessey, C.M., Jones, M.E., Taillefert, M., DiChristina, T.J., 2010. Anaerobic
900 production and respiration of soluble organic-Fe(III) by siderophore biosynthesis and
901 Fe(III)-siderophore reductase mutants of *Shewanella oneidensis*. App. Environ.
902 Microbiol. 76, 2425-2432.

903 Fischer, D., Sahling, H., Nothen, K., Bohrmann, G., Zabel, M., Kasten, S., 2012.
904 Interaction between hydrocarbon seepage, chemosynthetic communities, and bottom

905 water redox at cold seeps of the Makran accretionary prism: insights from
906 habitat-specific pore water sampling and modeling. Biogeosci. 9, 2013-2031.

907 Goffredi, S.K., Barry, J.P., 2002. Species-speci¢c variation in sulfide physiology between
908 closely related vesicomyid clams. Mar. Ecol. Prog. Series 225, 227-238.

909 Guillon, E., Menot, L., Decker, C., Krylova, E., Olu, K., 2017. The vesicomyid bivalve
910 habitat at cold seeps supports heterogeneous and dynamic macrofaunal assemblages.
911 Deep Sea Res. I 120, 1-13.

912 Jones, M., Fennessey, C.M., DiChristina, T.J., Taillefert, M., 2010. *Shewanella oneidensis*
913 MR-1 mutants selected for their inability to produce soluble organic-Fe(III) complexes
914 are unable to respire Fe(III) as anaerobic electron acceptor. Environ. Microbiol. 12,
915 938-950.

916 Jones, M.E., Beckler, J.S., Taillefert, M., 2011. The flux of soluble organic-iron(III)
917 complexes from sediments represents a source of stable iron(III) to estuarine waters
918 and to the continental shelf. Limnol. Oceanogr. 56, 1811-1823.

919 Jorgensen, B.B., 1982. Mineralization of organic matter in the sea bed - the role of sulfate
920 reduction. Nature 296, 643-645.

921 Hall, P.O.J., Aller, R.C., 1992. Rapid, small-volume, flow injection analysis for SCO2 and
922 NH4+ in marine and freshwaters. Limnol. Oceanogr. 37, 1113-1119.

923 Hedges, J.I., Keil, R.G., 1995. Sedimentary organic matter preservation: an assessment and
924 speculative synthesis. Mar. Chem. 49, 81-115.

925 Engler, R.M., Patrick, W.H., 1975. Stability of sulfides of manganese, iron, zinc, copper,
926 and mercury in flooded and non-flooded soil. Soil Sci. 119, 217-221.

927 Hales, B., Van Geen, A., Takahashi, T., 2004. High-frequency measurement of seawater
928 chemistry: Flow-injection analysis of macronutrients. Limnol. Oceanogr. Meth. 2,
929 91-101.

930 Henneke, E., Luther III, G.W., De Lange, G.J., 1991. Determination of inorganic sulphur
931 speciation with polarographic techniques: Some preliminary results for recent
932 hypersaline anoxic sediments. Mar. Geol. 100, 115-123.

933 Herszage, J., Dos Santos Afonso, M., 2003. Mechanism of hydrogen sulfide oxidation by
934 manganese(IV) oxide in aqueous solutions. Langmuir 19, 9684-9692.

935 Heyl, T.P., Gilhooly, W.P., Chambers, R.M., Gilchrist, G.W., Macko, S.A., Ruppel, C.D.,
936 Van Dover, C.L., 2007. Characteristics of vesicomyid clams and their environment at
937 the Blake Ridge cold seep, South Carolina, USA. Mar. Ecol. Prog. Ser. 339, 169-184.

938 Hoehler, T.M., Alperin, M.J., Albert, D.B., Martens, C.S., 2001. Apparent minimum free
939 energy requirements for methanogenic Archea and sulfate-reducing bacteria in an
940 anoxic marine sediment. FEMS Microbiol. Ecol. 38, 33-41.

941 Homoky, W.B., Hembury, D.J., Hepburn, L.E., Mills, R.A., Statham, P.J., Fones, G.R.,
942 Palmer, M.R., 2011. Iron and manganese diagenesis in deep sea volcanogenic
943 sediments and the origins of pore water colloids. Geochim. Cosmochim. Acta 75,
944 5032-5048.

945 Howarth, R.W., 1984. The ecological significance of sulfur in the energy dynamics of salt
946 marsh and coastal marine sediments. Biogeochem. 1, 5-27.

947 Huang, S., Jaffe, P.R., 2015. Characterization of incubation experiments and development
948 of an enrichment culture capable of ammonium oxidation under iron-reducing
949 conditions. Biogeosci. 12, 769-779.

950 Kostka, J.E., Luther III, G.W., 1994. Partitioning and speciation of solid phase iron in
951 saltmarsh sediments. Geochim. Cosmochim. Acta 58, 1701-1710.

952 Kostka, J.E., Wu, J., Nealson, K.H., Stucki, J.W., 1999. The impact of structural Fe(III)
953 reduction by bacteria on the surface chemistry of smectite clay minerals. Geochim.
954 Cosmochim. Acta 63, 3705-3713.

955 Kostka, J.E., Gribsholt, B., Petrie, E., Dalton, D., Skelton, H., Kristensen, E., 2002. The
956 rates and pathways of carbon oxidation in bioturbated saltmarsh sediments. Limnol.
957 Oceanogr. 47, 230-240.

958 Law, G.T.W., Shimmield, T.M., Shimmield, G.B., Cowie, G.L., Breuer, E.R., Harvey,
959 S.M., 2009. Manganese, iron, and sulphur cycling on the Pakistan Margin. Deep Sea
960 Res. II 56, 305-323.

961 Levesque, C., Limen, H., Juniper, S.K., 2005. Origin, composition and nutritional quality
962 of particulate matter at deep-sea hydrothermal vents on Axial Volcano, NE Pacific.
963 Mar. Ecol. Prog. Series 289, 43-52.

964 Levin, L.A., Ziebis, W., Mendoza, G.F., Growney, V.A., Tryon, M.D., Brown, K.M.,
965 Mahn, C., Gieskes, J.M., 2003. Spatial heterogeneity of macrofauna at northern
966 California methane seeps: influence of sulfide concentration and fluid flow. Mar. Ecol.
967 Prog. Ser. 265, 123-139.

968 Lin, S., Morse, J.W., 1991. Sulfate reduction and iron sulfide mineral formation in Gulf of
969 Mexico anoxic sediments. Amer. J. Sci. 291, 55-89.

970 Lowe, K.L., DiChristina, T.J., Roychoudhury, A.N., Van Cappellen, P., 2000.
971 Microbiological and geochemical characterization of microbial Fe(III) reduction in salt
972 marsh sediments. Geomicrobiol. J. 17, 163-178.

973 Luther III, G.W., Shellenbarger, P.A., Brendel, P.J., 1996. Dissolved organic Fe(III) and
974 Fe(II) complexes in saltmarsh porewaters. Geochim. Cosmochim. Acta 60, 951-960.

975 Luther III, G.W., Glazer, B.T., Ma, S., Trouwborst, R.E., Moore, T.S., Metzger, E., Kraiya,
976 C., Waite, T.J., Druschel, G., Sundby, B., Taillefert, M., Nuzzio, D.B., Shank, T.M.,
977 Lewis, B.L., Brendel, P.J., 2008. Use of voltammetric solid-state (micro)electrodes for
978 studying biogeochemical processes: Laboratory measurements to real time
979 measurements with an in situ electrochemical analyzer (ISEA). Mar. Chem. 108,
980 221-235.

981 Martens, C.S., Goldhaber, M.B., 1978. Early diagenesis in transitional sedimentary
982 environments of the White Oak River Estuary, North Carolina. Limnol. Oceanogr. 23,
983 428-441.

McManus, J., Berelson, W.M., Coale, K.H., Johnson, K.S., Kilgore, T.E., 1997. Phosphorus regeneration in continental margin sediments. Geochim. Cosmochim. Acta 61, 2891-2907.

Meiggs, D., Taillefert, M., 2011. The effect of riverine discharge on biogeochemical processes in estuarine sediments. Limnol. Oceanogr. 56, 1797-1810.

Millero, F.J., 1986. The thermodynamics and kinetics of hydrogen sulfide system in natural waters. Mar. Chem. 18, 121-127.

Millero, F.J., Tolongo, S., Izaguirre, M., 1987. The oxidation kinetics of Fe(II) in seawater. Geochim. Cosmochim. Acta 51, 793-801.

McKee, B.A., Aller, R.C., Allison, M.A., Bianchi, T.S., Kineke, G.C., 2004. Transport and transformation of dissolved and particulate materials on continental margins influenced by major rivers: Benthic boundary layer and seabed processes. Cont. Shelf Res. 24, 899-926.

Murphy, J., Riley, J.P., 1962. A modified single solution method for the determination of phosphate in natural waters. Anal. Chim. Acta. 27, 31-36.

Noffke, A., Hensen, C., Sommer, S., Scholz, F., Bohlen, L., Mosch, T., Graco, M., Wallmann, K., 2012. Benthic iron and phosphorus fluxes across the Peruvian oxygen minimum zone. Limnol. Oceanogr. 57, 851-867.

Olu, K., Decker, C., Pastor, L., Caprais, J.-C., Khripounoff, A., Morineaux, M., Ain Baziz, M., Menot, L., Rabouille, C., 2017. Cold-seep-like macrofaunal communities in

organic- and sulfide-1 rich sediments of the Congo deep-sea fan. Deep Sea Res II. This Issue.

Pastor, L., Cathalot, C., Deflandre, B., Viollier, E., Soetaert, K., Meysman, F.J.R., Ulses, C., Metzger, E., Rabouille, C., 2011. Modeling biogeochemical processes in sediments from the Rhone River prodelta area (NW Mediterranean Sea). Biogeosci. 8, 1351-1366.

Pastor, L., Toffin, L., Decker, C., Olu, K., Lesongeur, F., Caprais, J.-C., Bessette, S., Cathalot, C., Brandily, C., Taillefert, M., Rabouille, C., 2016. Early diagenesis in the sediments of the Congo deep-sea fan dominated by massive terrigenous deposits: Part II - methane/sulfate interactions. Deep Sea Res. II. This issue.

Peiffer, S., dos Santos Afonso, M., Wehrli, B., Gachter, R., 1992. Kinetics and mechanism of the reaction of H_2S with Lepidocrocite. Environ. Sci. Technol. 26, 2408-2413.

Pozzato, L., Rabouille, C., Cathalot, C., Berrached, C., Toussaint, F., Stetten, E., Caprais, J.-C., Pastor, L., Olu, K., 2016. Early diagenesis in the Congo deep-sea fan sediments dominated by massive terrigenous deposits: Part I - Oxygen consumption and organic carbon mineralization using a micro-electrode approach. Deep Sea Res. II. This issue.

Pruski, A.M., Decker, C., Stetten, E., Vetion, G., Martinez, P., Charlier, K., Senyarich, C., Olu, K., 2016. Energy transfer in the Congo turbiditic system: from terrestrially-derived organic matter to chemosynthetic food webs. Deep Sea Res. II. This issue.

1024 Pyzik, A.J., Sommer, S.E., 1981. Sedimentary ion monosulfides: kinetics and mechanism
1025 of formation. Geochim. Cosmochim. Acta 45, 687-698.

1026 Rabouille, C., Caprais, J.-C., Lansard, B., Crassous, P., Dedieu, K., Reyss, J.L.,
1027 Khripounoff, A., 2009. Organic matter budget in the southeast atlantic continental
1028 margin close to the Congo canyon: In situ measurements of sediment oxygen
1029 consumption. Deep-Sea Res. II 56, 2223-2238.

1030 Rabouille, C., 2011. CONGOLOBE oceanographic cruise, R/V Pourquoi Pas?
1031 http://dx.doi.org/10.17600/11030170.

1032 Rickard, D., 1995. Kinetics of FeS precipitation: Part 1. Competing reaction mechanisms.
1033 Geochim. Cosmochim. Acta 59, 4367-4379.

1034 Rickard, D., Luther III, G.W., 1997. Kinetics of pyrite formation by the H_2S oxidation of
1035 iron(II) monosulfide in aqueous solutions between 25 and 125ºC: the mechanism.
1036 Geochim. Cosmochim. Acta 61, 135-147.

1037 Rickard, D., Oldroyd, A., Cramp, A., 1999. Voltammetric evidence for soluble FeS
1038 complexes in anoxic estuarine muds. Estuaries 22, 693-701.

1039 Rickard, D., 2006. The solubility of FeS. Geochim. Cosmochim. Acta 70, 5779-5789.

1040 Ristova, P.P., Wenzhofer, F., Ramette, A., Fischer, D., Kasten, S., Boetius, A., 2012.
1041 Bacterial diversity and biogeochemistry of different chemosynthetic habitats of the
1042 REGAB cold seep (West African margin, 3160m water depth). Biogeosci. 9,
1043 5031-5048.

1044 Roden, E.E., 2003. Fe(III) oxide reactivity toward biological versus chemical reduction.
1045 Environ. Sci. Technol. 37, 1319-1324.

1046 Sassen, R., Roberts, H.H., Aharon, P., Larkin, J., Chinn, E.W., Carney, R., 1993.
1047 Chemosythetic bacterial mats at cold hydrocarbon seeps, Gulf of Mexico
1048 continental-slope. Org. Geochem. 20, 77-89.

1049 Sen, A., Dennielou, B., Tourolle, J., Arnaubec, A., Rabouille, C., Olu, K., 2016. Fauna and
1050 habitat types in the turbidity current driven Congo deep-sea fan lobes. Deep Sea Res. II.
1051 This issue.

1052 Severmann, S., McManus, J., Berelson, W.M., Hammond, D.E., 2010. The continental
1053 shelf benthic iron flux and its isotope composition. Geochim. Cosmochim. Acta 74,
1054 3984-4004.

1055 Skoog, D.A., Leary, J.L., 1996. Principles of instrumental analysis, 4 ed. Saunders College
1056 Publishing.

1057 Stetten, E., Baudin, F., Reyss, J.L., Martinez, P., Charlier, K., Schnyder, J., Rabouille, C.,
1058 Dennielou, B., Coston-Guarini, J., Prusky, A., 2015. Organic matter characterization
1059 and distribution in sediments of the terminal lobes of the Congo deep-sea fan: Evidence
1060 for the direct influence of the Congo River. Mar. Geol. 369, 182-195.

1061 Stookey, L.L., 1970. Ferrozine: a new spectrophotometric reagent for iron. Anal. Chem.
1062 42, 779-781.

1063 Strickland, J.D.H., Parsons, T.R., 1972. A Practical Handbook of Seawater Analysis.
1064 Fisheries Research Board of Canada.

1065 Sung, W., Morgan, J.J., 1980. Kinetics and product of ferrous iron oxygenation in aqueous
1066 systems. Environ. Sci. Technol. 14, 561-568.

1067 Taillefert, M., Bono, A.B., Luther III, G.W., 2000a. Reactivity of Freshly Formed Fe(III)
1068 in Synthetic Solutions and (Pore)Waters: Voltammetric Evidence of an Aging Process.
1069 Environ. Sci. Technol. 34, 2169-2177.

1070 Taillefert, M., Luther III, G.W., Nuzzio, D.B., 2000b. The Application of Electrochemical
1071 Tools for In-Situ Measurements in Aquatic Systems: A Review. Electroanal. 12,
1072 401-412.

1073 Taillefert, M., Hover, V.C., Rozan, T.F., Theberge, S.M., Luther III, G.W., 2002. The
1074 influence of sulfides on soluble organic-Fe(III) in anoxic sediment porewaters.
1075 Estuaries 25, 1088-1096.

1076 Taillefert, M., Beckler, J.S., Carey, E.A., Burns, J.L., Fennessey, C.M., DiChristina, T.J.,
1077 2007. *Shewanella putrefaciens* produces an Fe(III)-solubilizing ligand during
1078 anaerobic respiration on insoluble Fe(III) oxides J. Inorg. Biochem. 101, 1760-1767.

1079 Tebo, B.M., Bargar, J.R., Clement, B.G., Dick, G.J., Murray, K.J., Parker, D., Verity, R.,
1080 Webb, S.M., 2004. Biogenic manganese oxides: Properties and mechanisms of
1081 formation. Ann. Rev. Earth Planet. Sci. 32, 287-328.

1082 Tercier-Waeber, M.-L., Taillefert, M., 2008. Remote in situ voltammetric techniques to
1083 characterize the biogeochemical cycling of trace metals in aquatic systems. J. Environ.
1084 Monitor. 10, 30-54.

1085 Thamdrup, B., Canfield, D.E., 1996. Pathways of carbon oxidation in continental margin
1086 sediments off central Chile. Limnol. Oceanogr. 41, 1629-1650.

1087 Theberge, S.M., Luther III, G.W., 1997. Determination of the electrochemical properties of
1088 a soluble aqueous FeS species present in sulfidic solutions. Aqua. Geochem. 3,
1089 191-211.

1090 Ullman, W.J., Aller, R.C., 1982. Diffusion coefficients in nearshore marine sediments.
1091 Limnol. Oceanogr. 27, 552-556.

1092 Van der Zee, C., Raaphorst, W.v., Helder, W., 2002. Fe redox cycling in Iberian
1093 continental margin sediments (NE Atlantic). J. Mar. Res. 60, 855-886.

1094 Wehrmann, L.M., Formolo, M.J., Owens, J., Raiswell, R., Ferdelman, T.G., Riedinger, N.,
1095 Lyons, T.W., 2014. Iron and manganese speciation and cycling in glacially influenced
1096 high-latitude fjord sediments (West Spitsbergen, Svalbard): Evidence for a benthic
1097 recycling-transport mechanism. Geochim. Cosmochim. Acta 141, 628-655.

1098 Wenzhofer, F., Greeff, O., Riess, W., 2002. Benthic carbon mineralization in sediments of
1099 Gotland Basin, Baltic Sea, measured in situ with benthic landers, in: Taillefert, M.,
1100 Rozan, T.F. (Eds.), Environmental Electrochemistry: analyses of trace element
1101 biogeochemistry. American Chemical Society, Washington D.C., pp. 162-185.

1102 Zinder, B., Furrer, G., Stumm, W., 1986. The coordination chemistry of weathering: II.
1103 Dissolution of Fe(III) oxides. Geochim. Cosmochim. Acta 50, 1861-1869.

1104 8.0 Figures

1105 Figure 1. Maps of the stations in the Congo River Fan, including the high resolution
1106 bathymetry obtained at the site during the same cruise (courtesy of Laurence Droz,
1107 ©Ifremer, Congolobe cruise).

1108 Figure 2. Depth profiles of $O_{2(aq)}$, Mn^{2+}, Fe^{2+} (first quadrant), organic-Fe(III), $FeS_{(aq)}$ (second
1109 quadrant), poorly crystalline and crystalline Fe(III) oxides (third quadrant), and Fe^{2+},
1110 dissolved Fe(III), and ΣPO_4^{3-} (fourth quadrant) on the levees of: a) Site A (MTB 2 core); b)
1111 Site F (MTB 5 core); c) Site C (MTB 6 core); d) Site B (MTB 12 core); and e) Site E (MTB
1112 14 core).

1113 Figure 3. Depth profiles of $O_{2(aq)}$, Mn^{2+}, Fe^{2+}, ΣH_2S (first quadrant), organic-Fe(III), $FeS_{(aq)}$,
1114 and pH (second quadrant) measured electrochemically: a) outside (push core
1115 CoLA-PL484-CT3); and b) inside (push core CoLA-PL484-CT10) the habitats of Site A
1116 colonized by *Vesicomyidae* species during dive # PL484. Solid FeS (third quadrant) and
1117 DIC and ΣPO_4^{3-} obtained after pore water extractions are also shown for the inside core
1118 (fourth quadrant). c) Picture of the *Vesicomyidae* habitat taken by the ROV Victor 6000
1119 during sampling with push cores inserted in the sediment.

1120 Figure 4. Depth profiles of $O_{2(aq)}$, Mn^{2+}, Fe^{2+}, ΣH_2S (first quadrant), organic-Fe(III), $FeS_{(aq)}$,
1121 pH (second quadrant) measured electrochemically, as well as DIC and ΣPO_4^{3-} (third
1122 quadrant) after pore water extractions: a) about 30 cm outside (push core PL491-CT16);

and b) inside (push core PL491-CT7) of a reduced patch of sediment colonized by *Vesicomyidae* species at Site C during dive # PL491. c) Picture of the *Vesicomyidae* habitat taken by the ROV Victor 6000 during sampling.

Figure 5. a) Picture of a reduced sediment at Site C obtained by the ROV Victor 6000 during dive # PL490. b) Depth profiles of $O_{2(aq)}$, Mn^{2+}, Fe^{2+}, ΣH_2S (first quadrant), organic-Fe(III), $FeS_{(aq)}$, pH (second quadrant) measured electrochemically, as well as solid FeS (third quadrant), NH_4^+, DIC, and ΣPO_4^{3-} (fourth quadrant) after pore water extractions of push core PL490-CT20 from the middle of the reduced sediment. Zones were data were not obtained either due to the lack of pore waters or sample loss are labeled 'No Data'.

Figure 6. a) Picture of a white microbial mat at Site C obtained by the ROV Victor 6000 during dive # PL490. b) Depth profiles of $O_{2(aq)}$, Mn^{2+}, Fe^{2+}, $S_2O_3^{2-}$, ΣH_2S (first quadrant) and organic-Fe(III), $FeS_{(aq)}$, and pH (second quadrant) measured electrochemically in push core PL490-CT2.

Figure 7. Correlation between organic-Fe(III) complexes and Fe^{2+} measured electrochemically in the sediments collected from the levees at Site A, Site B, Site C, CoLE, and Site F. The positive correlation between organic-Fe(III) and Fe^{2+} ($R^2 = 0.751$) suggests that organic-Fe(III) complexes are produced as intermediate during the microbial reduction of Fe(III) oxides, given the high Fe(III) oxide content of these sediments, that dissolved sulfide was never detected in the pore waters of any of these sediment cores, and that organic-Fe(III) is extremely rapidly reduced by dissolved sulfides.

1143 Figure 8. Schematic diagram of the pore water geochemical composition in the
1144 background sediment (left) and the discrete habitats (right) along the active channel of the
1145 Congo deep-sea fan. The lower panel depicts the geochemical composition of the pore
1146 waters across a lateral section from the background sediment to the habitats. It displays the
1147 sharp boundary observed that is maintained by "FeS titration" (see text for details).

1148 Figure 9. Correlation between total dissolved sulfide (ΣH_2S) and dissolved: a) Mn^{2+}; and b)
1149 Fe^{2+} measured electrochemically as a function of depth in the sediments of the levees and
1150 the main channel at Site A, Site B, Site C, Site E, and Site F. The lines display the
1151 stoichiometric relationship between dissolved sulfide and a) Mn^{2+}(1:1) or b) Fe^{2+} (1:2) if
1152 the reduced metals were only produced via abiotic reduction of their metal oxides by
1153 dissolved sulfide. Any data above the lines indicate excess sulfate reduction, while data
1154 below the lines indicate excess metal reduction. Most of the channel samples fall above the
1155 lines, suggesting reduced metals are mainly produced during abiotic reduction of Mn(IV)
1156 oxides and Fe(III) oxides. In turn, all the levees samples fall below the line, suggesting
1157 microbial metal reduction is responsible for the production of these species.

1158 Figure 10. Percent carbon remineralization attributed to denitrification, dissimilatory
1159 Mn(IV)-, Fe(III)-, and sulfate-reduction in the sediments collected from the: a) levees; and
1160 b) discrete habitats along the Congo River deep-sea fan active channel. Total carbon
1161 remineralization was estimated from dissolved oxygen uptake (DOU) fluxes. Although
1162 denitrification and dissimilatory Fe(III) reduction dominates anaerobic respiration in levee
1163 sediments, aerobic respiration accounts for the majority of carbon remineralization rates.
1164 In turn, anaerobic processes are so intense in the discrete habitats that the production of

1165 sulfide is in excess of aerobic respiration. These findings indicate that the discrete habitats
1166 are dominated by sulfate reduction and that the fluxes of Mn^{2+} and Fe^{2+} are likely due to
1167 abiotic reduction of Mn(IV) and Fe(III) oxides by total dissolved sulfides.

Figure

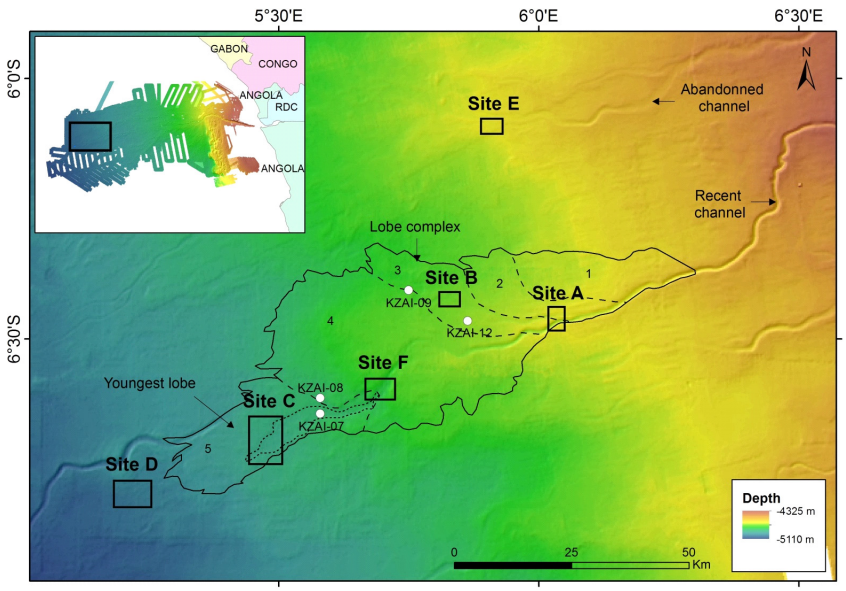

Figure 1. - Taillefert et al., 2016

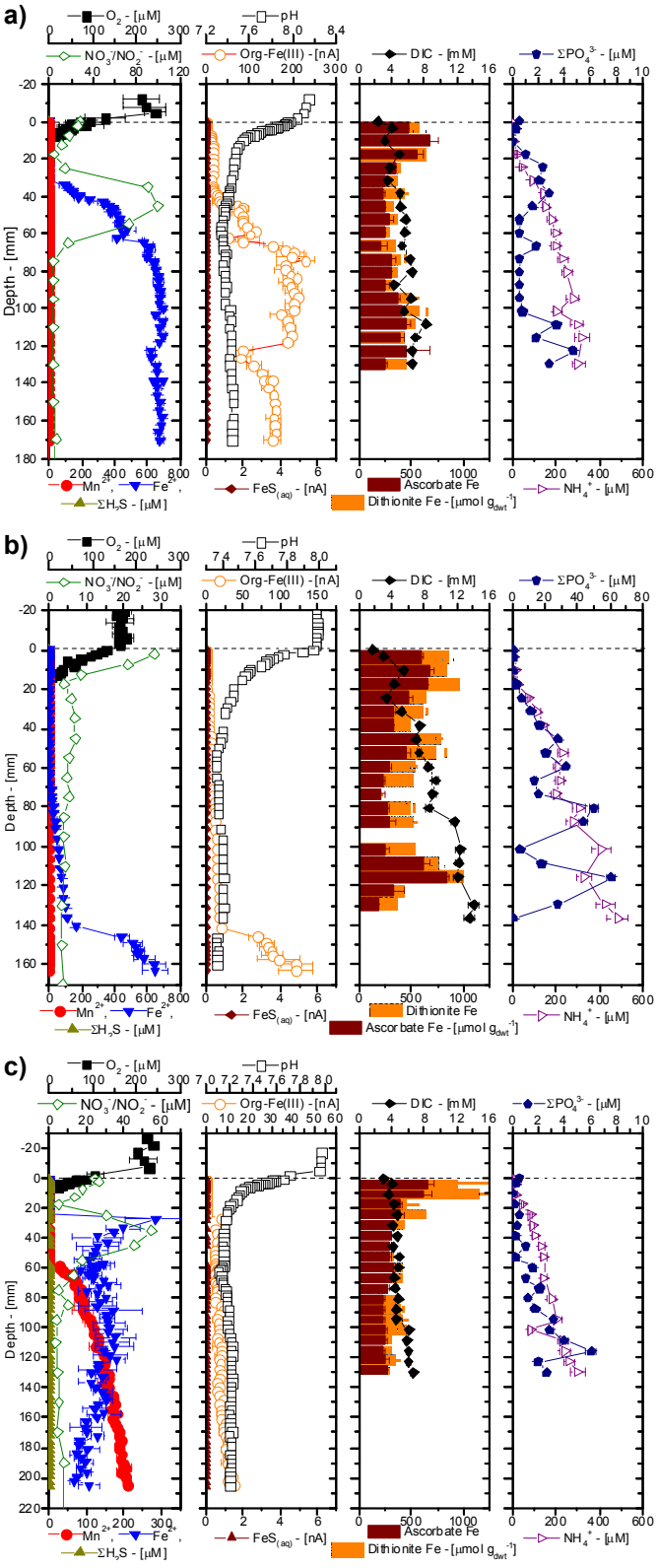

Figure 2. - Taillefert et al., 2016

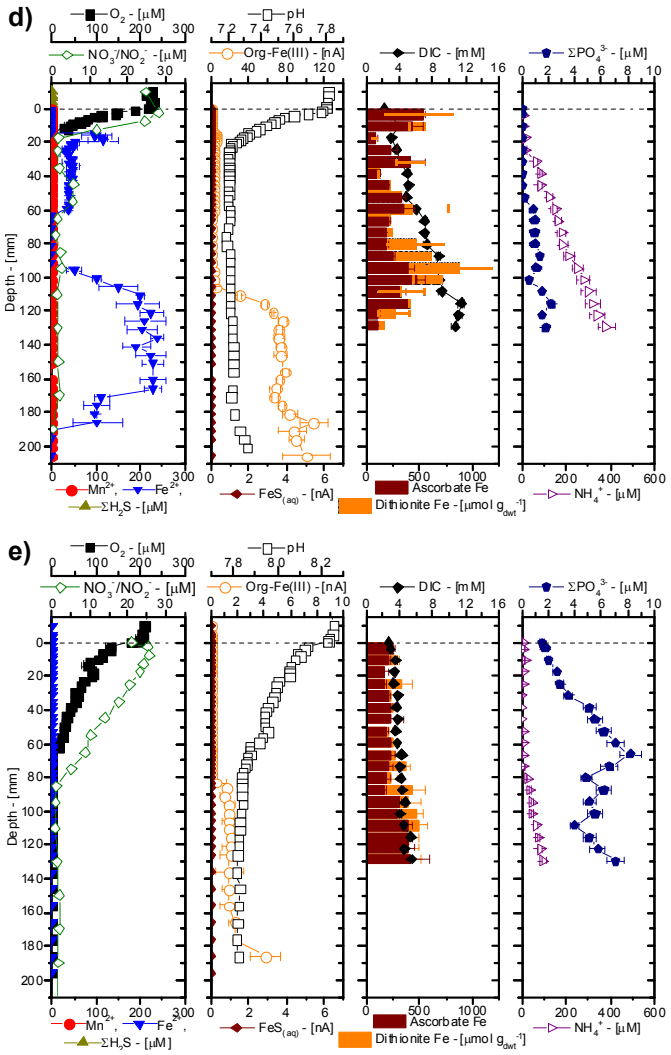

Figure 2 (Cont.) - Taillefert et al., 2016

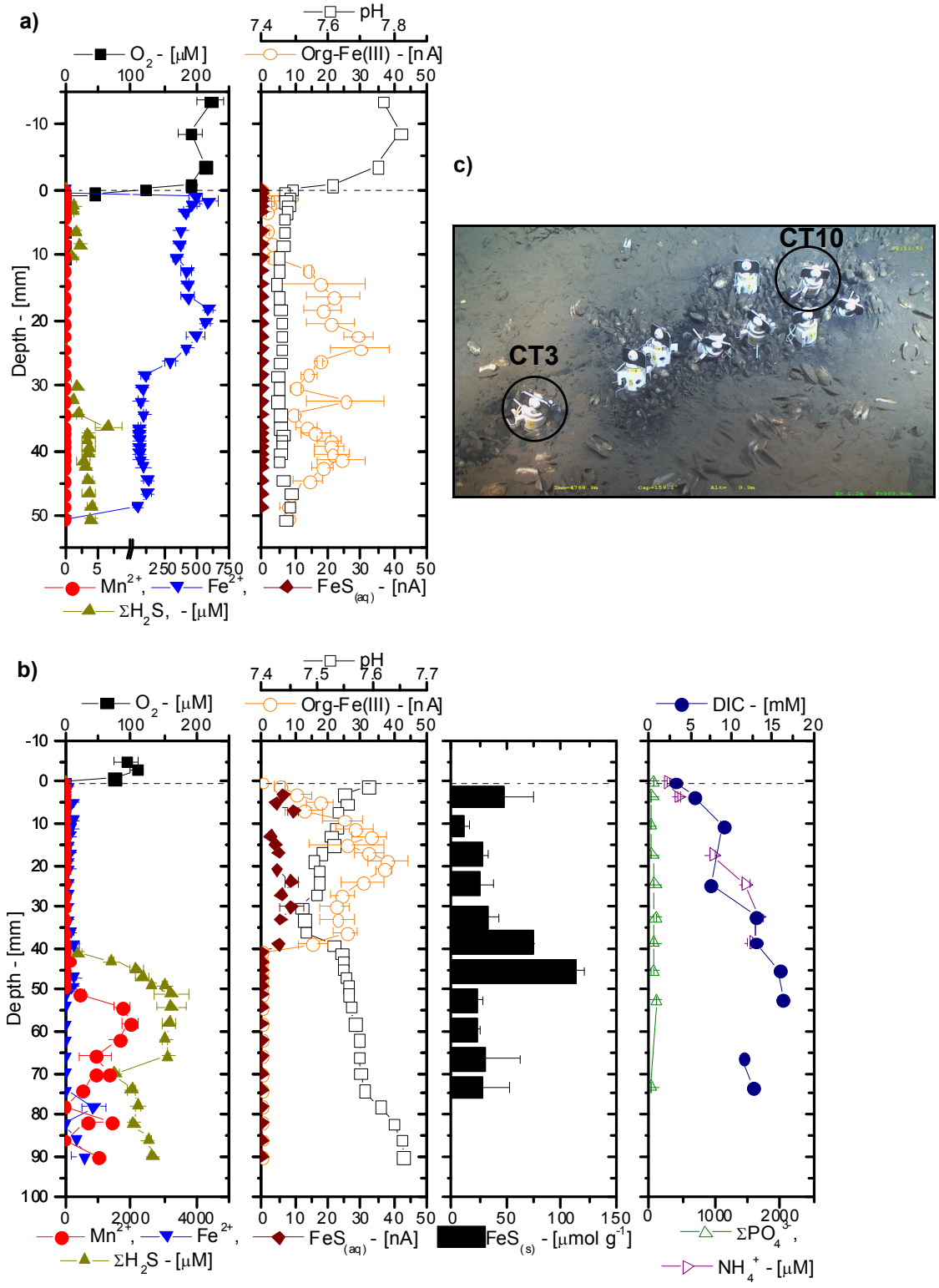

Figure 3. - Taillefert et al., 2016

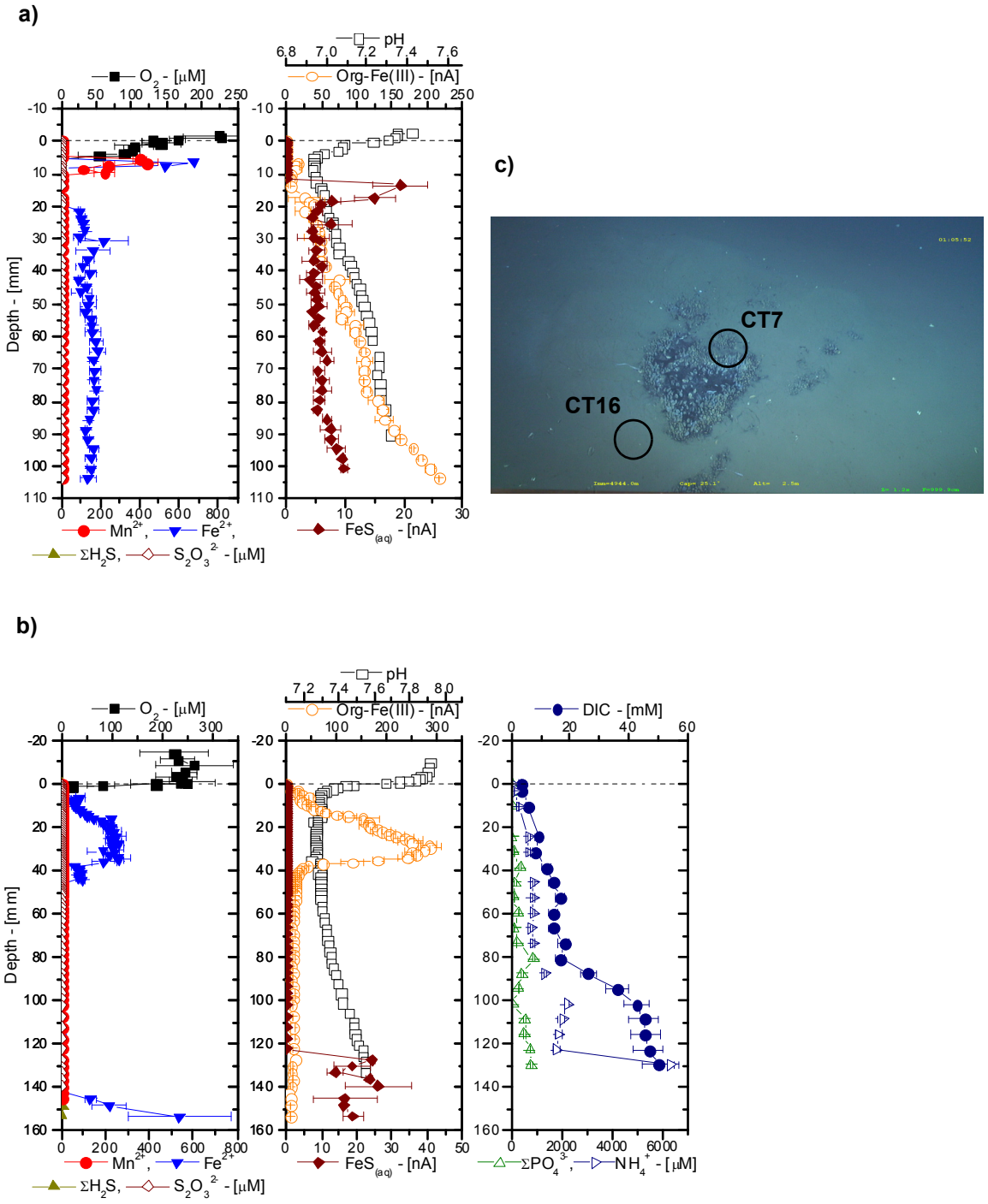

Figure 4. - Taillefert et al., 2016

a)

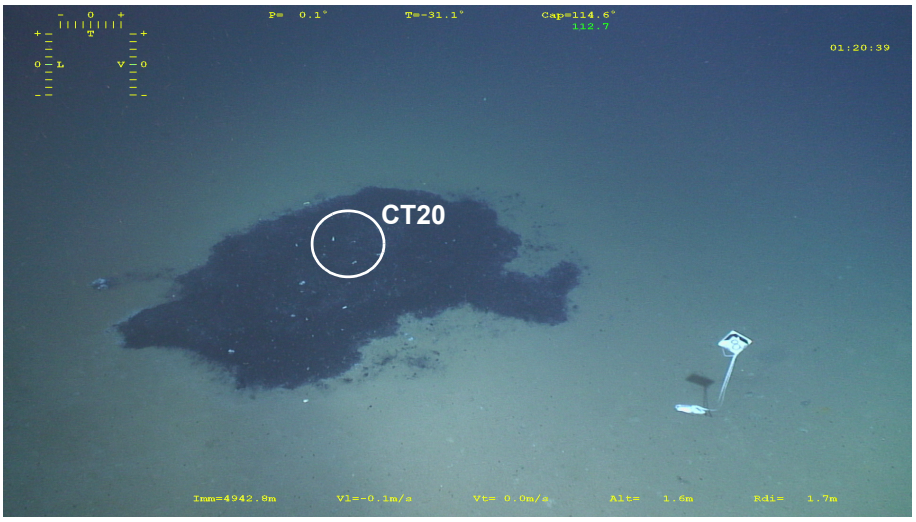

b)

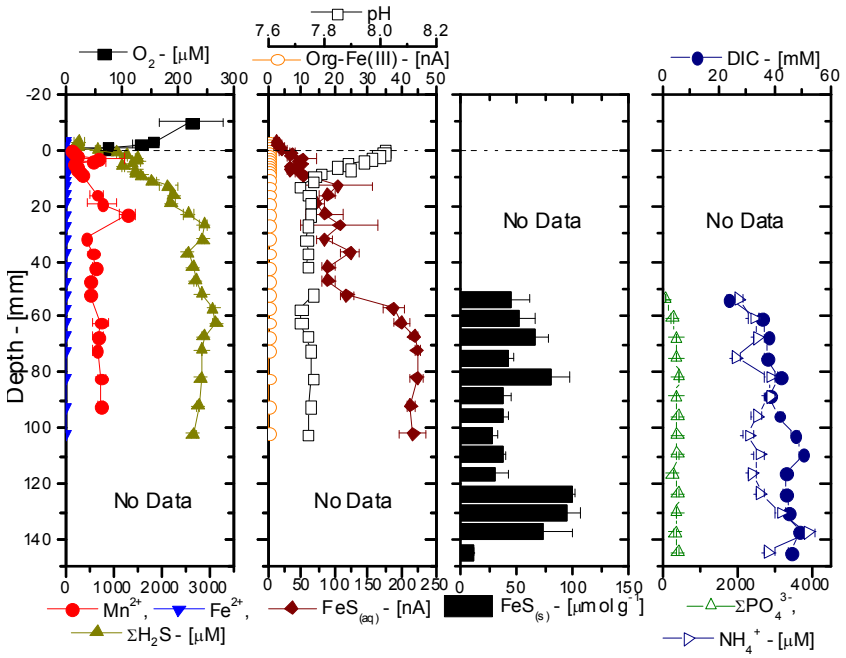

Figure 5. - Taillefert et al., 2016

a)

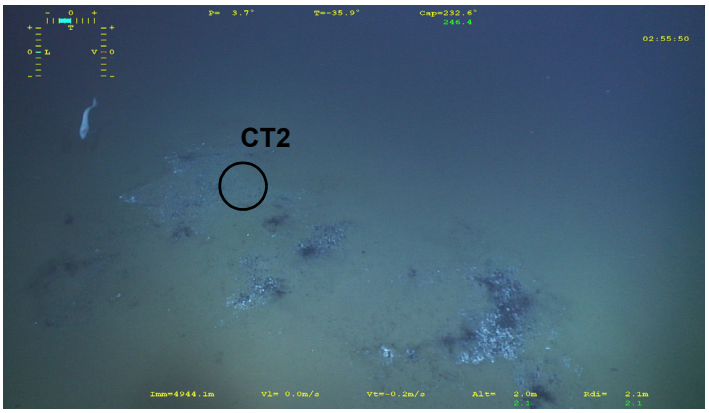

b)

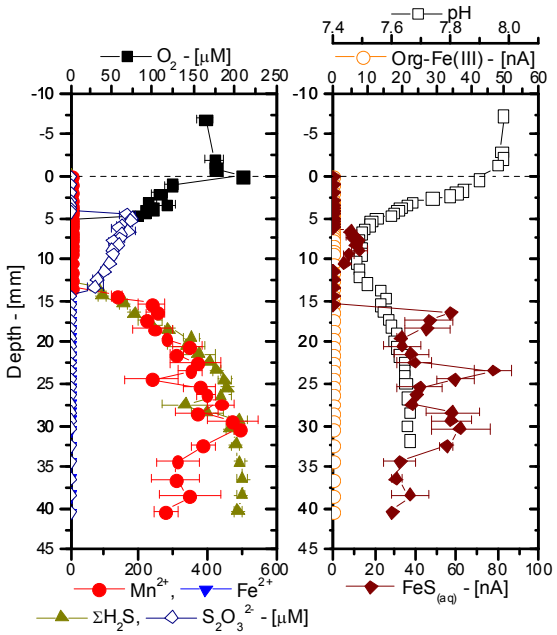

Figure 6. - Taillefert et al., 2016

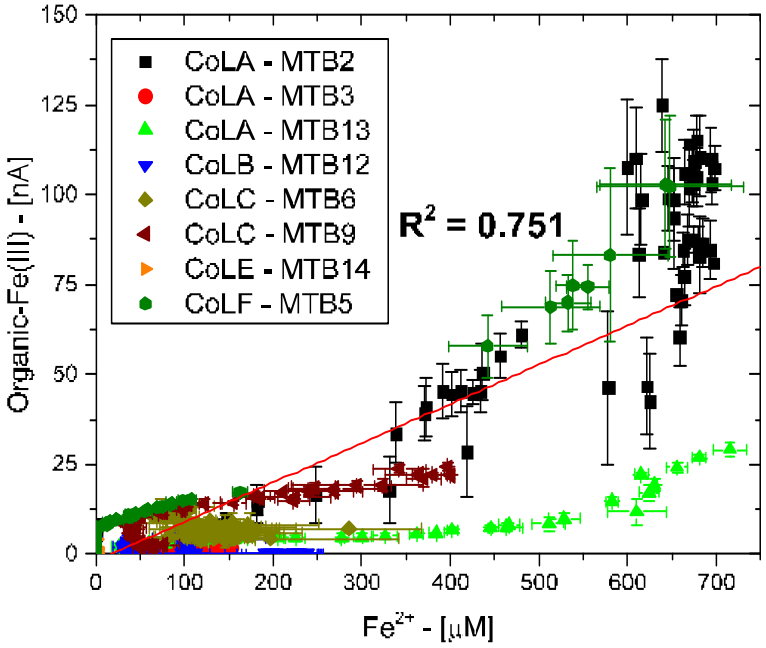

Figure 7. - Taillefert et al., 2016

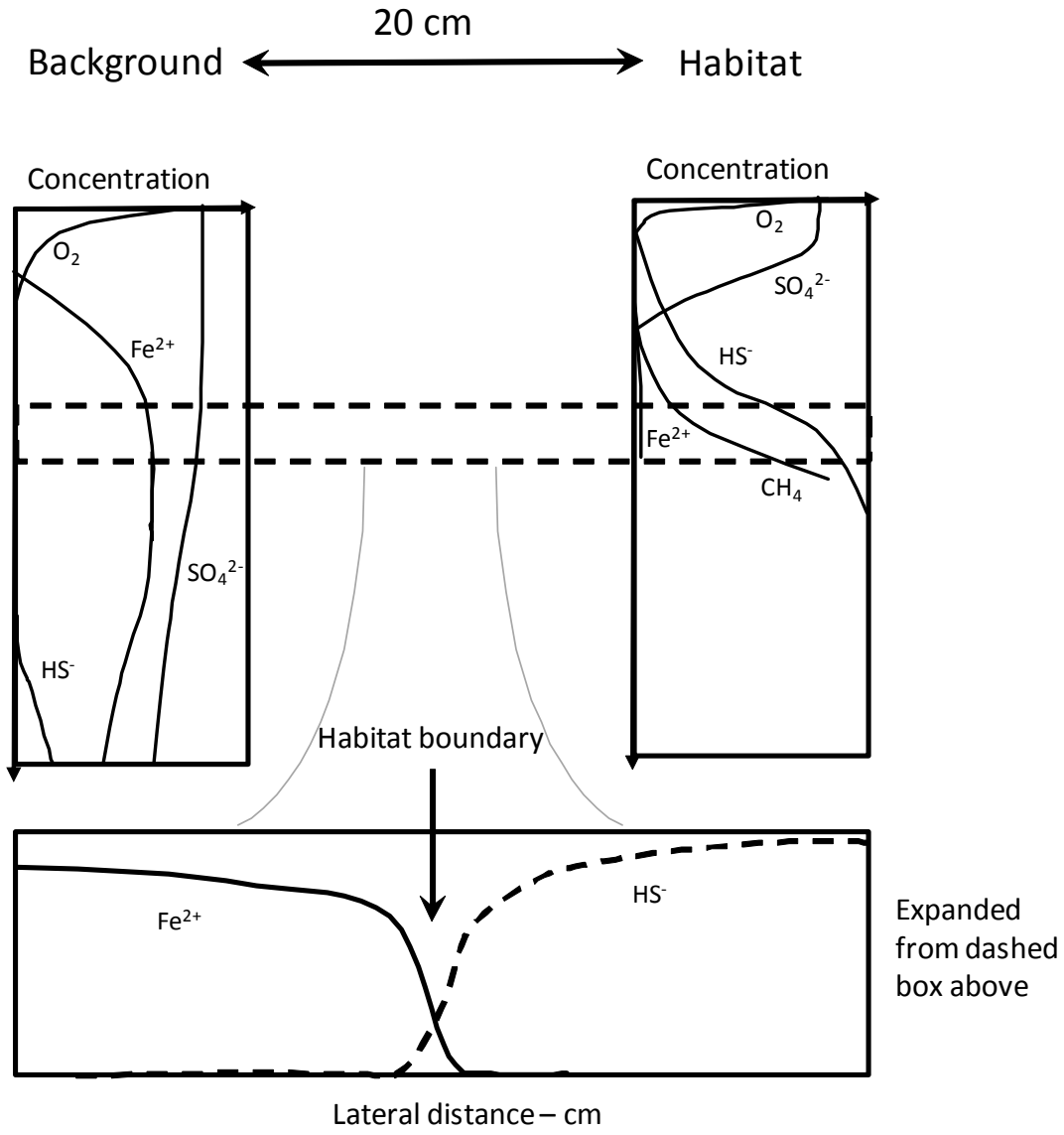

Figure 8. - Taillefert et al., 2016

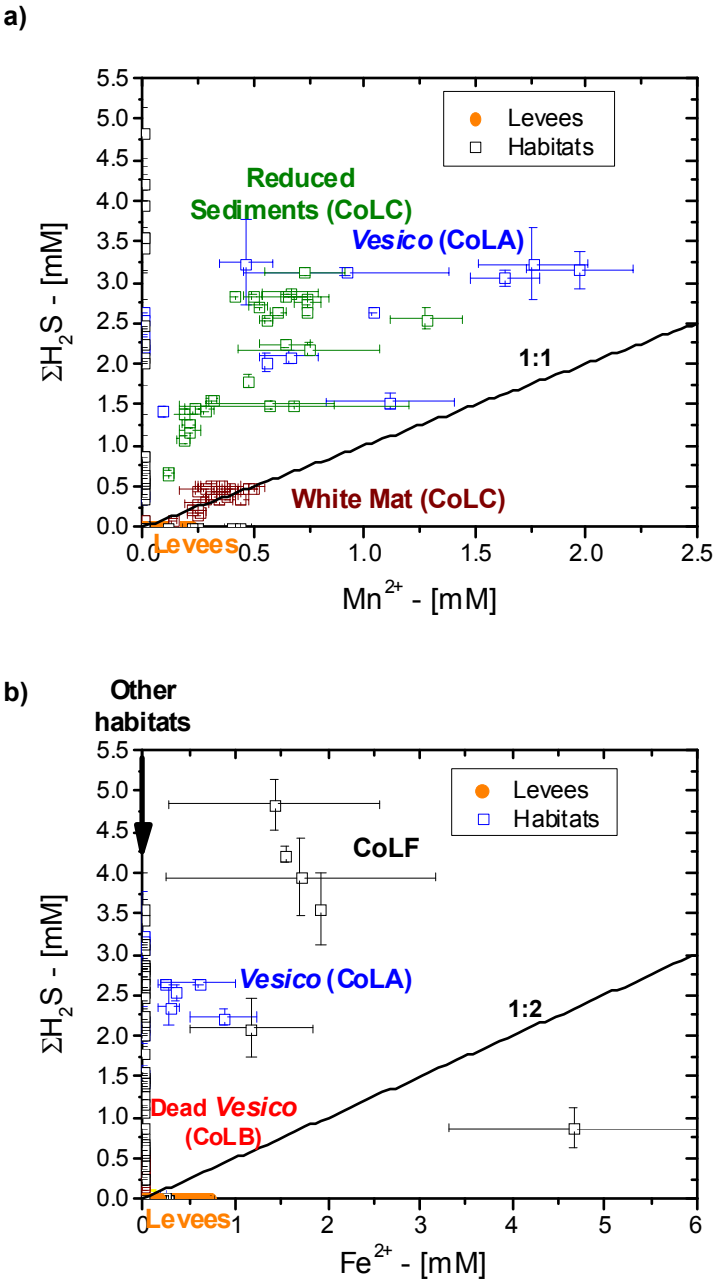

Figure 9. - Taillefert et al., 2016

a)

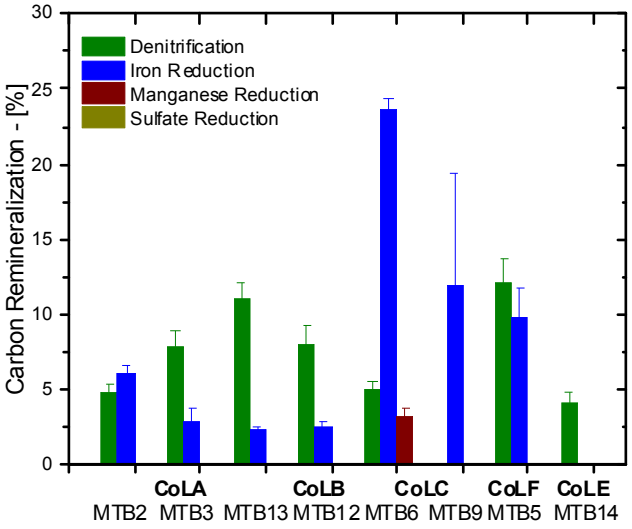

b)

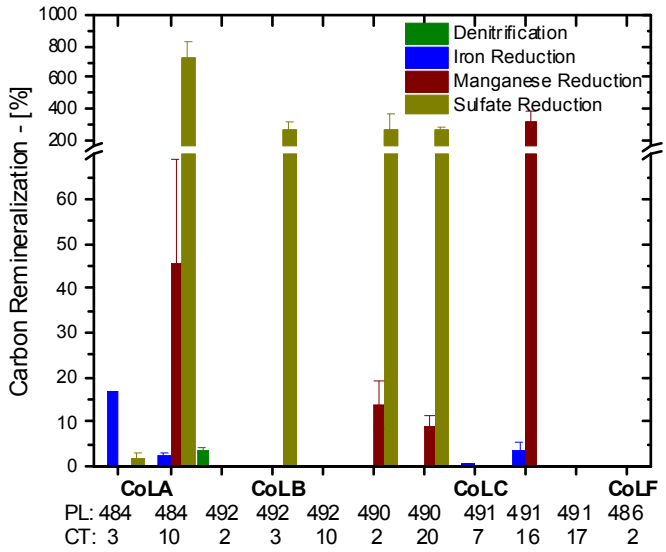

Figure 10. - Taillefert et al., 2016

9.0 Tables

Table 1. Location, water depth (m), and description of the stations where sediments were collected along the Congo River deep-sea fan using a multi-corer (MTB-#) or push cores (CT#) with the ROV Victor 6000. PL### corresponds to the dive number of the ROV (see complete list and pictures in Rabouille et al., this issue).

Station	Location	Depth	Core	Habitat description
Site A	6°27'35.92"S; 6°2'4.74"E	4759	MTB-2	Northern levee
	6°28'12.57"S; 6°2'12.99"E	4764	MTB-3	Southern channel flank
	6°28'16.70"S; 6°2'8.71"E	4769	PL484-CT3	Outside less dense patch of *Vesicomyidae*
	6°28'16.54"S; 6°2'9.07"E	4769	PL484-CT10	Inside less dense patch of *Vesicomyidae*
Site B	6°25'36.96"S; 5°49'35.25"E	4823	MTB-12	In the abandoned channel, near southern flank
	6°25'14.86"S; 5°49'42.45"E	4718	PL492-CT2	Edge of scattered patch of dead *Vesicomyidae*
	6°25'14.60"S; 5°49'42.57"E	4718	PL492-CT3	Inside scattered patch of dead *Vesicomyidae*
	6°25'13.00"S; 5°49'42.91"E	4718	PL492-CT10	Outside scattered patch of dead *Vesicomyidae*
Site C	6°40'15.95"S; 5°28'24.06"E	4951	MTB-6	Northern levee, ~600 m from channel, near MTB-9
	6°40'16.08"S; 5°28'25.63"E	4950	MTB-9	Northern levee, ~600 m from channel, near MTB-6
	6°41'23.59"S; 5°28'45.94"E	4946	PL490-CT2	White microbial mat
	6°40'57.00"S; 5°28'55.18"E	4844	PL490-CT20	Deeply reduced black sediment free of megafauna
	6°42'05.12"S; 5°29'17.58"E	4846	PL491-CT7	Edge of dense patch of *Vesicomyidae*
	6°42'05.06"S; 5°29'16.87"E	4846	PL491-CT16	Outside dense patch of *Vesicomyidae*
	6°42'13.15"S; 5°29'19.43"E	4846	PL491-CT17	Orange microbial mat
Site E	6°5'53.64"S; 5°54'29.07"E	4750	MTB-14	Main channel bank
Site F	6°34'50.08"S; 5°41'27.99E	4864	MTB-5	Levee, ~500 m from channel

Table 2. Saturation index of mackinawite calculated from ΣH_2S, Fe^{2+}, and pH data in the levees and in the channel at each station along the Congo River fan. The saturation index was negative in all the levee sediments and most of the channel sediments.

Site	Core	Depth (mm)	Saturation Index
Site A	PL484 - CT3	2.4 - 10.4	1.39 - 2.24
		30.4 - 48.5	0.03 - 1.43
	PL484 - CT10	47 - 49	9.00 - 9.01
		78 - 90	9.65 - 10.32
Site C	PL491 - CT7	148.2	3.0

13

Table 3. C:N ratio estimated from dissolved inorganic carbon (DIC) and ammonium concentrations, and diffusive fluxes of dissolved oxygen, DIC, ammonium, nitrate, Mn^{2+}, Fe^{2+}, and total dissolved sulfide in the pore waters of the levees and discrete habitat sediments. Except for site E, nitrate fluxes in the levee sediments were obtained from the top two centimeters of the sediment only. Diffusive fluxes of each species were calculated using at least four points along the profiles. Numbers in parenthesis represent the standard deviation of the fluxes. N/A = not applicable.

Station	Core	C:N Ratio	Diffusive Flux - [mmol m^{-2} d^{-1}]						
			$O_{2(aq)}$	DIC	NH_4^+	NO_3^-	Mn^{2+}	Fe^{2+}	ΣH_2S
Levees									
Site A	MTB-2	5.7(1.0)	-2.69(0.19)	1.68(0.27)	0.37(0.05)	-0.11(0.01)	0	0.65(0.04)	0
	MTB-3	7.0(1.1)	-1.19(0.08)	2.77(0.32)	0.22(0.01)	-0.07(0.01)	0	0.14(0.04)	0
Site F	MTB-5	12.9(1.1)	-1.28(0.07)	4.08(0.92)	0.33(0.03)	-0.12(0.02)	0	0.5(0.09)	0
Site C	MTB-6	4.8(1.0)	-2.64(0.07)	1.33(0.48)	0.22(0.01)	-0.11(0.01)	0.08(0.01)	2.51(0)	0
	MTB-9	12.7(1.2)	-1.69(0.17)	3.98(0.85)	0.33(0.02)	N/A	0	0.81(0.5)	0
Site B	MTB-12	12.4(0.6)	-2.17(0.20)	2.41(0.29)	0.24(0.02)	-0.14(0.02)	0	0.22(0.02)	0
Site E	MTB-14	10.4(1.6)	-0.69(0.11)	1.13(0.34)	0.11(0.01)	-0.02(0.00)	0	0	0
Habitats									
Site A	PL484-CT3	N/A	-6.49(0.13)	N/A	N/A	N/A	0	4.31(0)	0.06(0.03)
	PL484-CT10	4.8(0.7)	-5.75(0.10)	9.42(3.24)	2.37(0.19)	0	5.25(2.7)	0.52(0.2)	21.2(2.55)
Site C	PL490-CT2	N/A	-2.83(0.96)	N/A	N/A	N/A	0.79(0.15)	0	3.77(0.17)
	PL490-CT20	4.3(1.9)	-5.14(0.27)	14.8(2.63)	1.5(0.85)	N/A	0.95(0.22)	0	6.61(0.57)
	PL491-CT7	12.6(0.9)	-12.3(1.0)	10.0(0.86)	1.19(0.16)	N/A	0	0.35(0.03)	0
	PL491-CT16	N/A	-1.60(0.24)	N/A	N/A	N/A	10.19(0)	0.22(0.14)	0
	PL491-CT17	3.3(1.2)	-2.11(0.26)	16.9(12.9)	1.02(0.43)	0	0	0	0
Site B	PL492-CT2	4.3(0.5)	N/A	2.33(0.62)	0.35(0.04)	0	N/A	N/A	N/A
	PL492-CT3	11.9(1.9)	-2.87(0.45)	2.24(1.22)	0.23(0.02)	N/A	0	0	3.85(0.34)
	PL492-CT10	N/A	-3.36(0.56)	N/A	N/A	N/A	0	0	0

14